NTNU – Trondheim
Norwegian University of
Science and Technology

Estimation of harmonic signatures in underwater noise from small boats

Ole Gunnar Mathisen Faltin

Master of Science in Electronics
Submission date: June 2015
Supervisor: Hefeng Dong, IET
Co-supervisor: Dag Tollefsen, Forsvarets forskningsinstitutt

Norwegian University of Science and Technology
Department of Electronics and Telecommunications

An expert is a person who has found out by
his own painful experience all the mistakes
that one can make in a very narrow field.
- Niels Bohr

Acknowledgements

I wish to thank my supervisor Professor Hefeng Dong at NTNU (Norwegian University of Science and Technology) for her much appreciated support. I also wish to thank my co-supervisor Dag Tollefsen at FFI (Norwegian Defence Research Establishment) the for the amazing job he has done to support and help me during my thesis work. I want to thank everyone involved at FFI for their help along the way, and the opportunity to conduct my thesis work for them.

I would also like to thank my family and friends for their patience and support during my thesis work.

Abstract

This thesis explores underwater noise from small boats. There has been an increased focus on anthropogenic noise in the marine environment within the EU in the past years. The focus of the thesis is to study the noise from the engines and propellers of small boats, which is in general composed of both a harmonic series, and broadband noise.

In this thesis, we apply two fundamental frequency estimators to a dataset consisting of noise recorded in the waters outside *Vealøs* in order to extract the harmonic signature of small vessels. We will explore estimators based upon the Non-linear Least Squares method and Capons method, which can calculate the fundamental frequency of harmonic noise in water. The estimators are adapted in order to suit the dataset and evaluated based on accuracy and computation time. Results show that the Capon estimator excels in performance at lower signal to noise ratio with a slight advantage, but that it comes at a cost; the Non-Linear Least Squares estimator has approximately one sixth of the Capon estimators computation time. Since the estimator based on Non-linear Least Squares method has so much lower computation time, this estimator is certainly favourable as this fact opens possibilities for an increased number of samples with lower or comparable computation time.

Sammendrag

I denne masteroppgaven utforsker vi undervannsstøy fra små båter. De siste årene har det vært økt fokus på antropogen støy i det marine miljø innenfor EU. Fokuset i oppgaven er på støy fra motoren og propellen til små båter, som består av en harmonisk rekke og bredbåndet støy.

I masteroppgaven bruker vi to fundamentalfrekvens estimatorer på et datasett bestående av støyopptak fra små båter tatt i vannet utenfor *Vealøs* for å finne den harmoniske signaturen til små fartøy. Vi vil utforske estimatorer basert på henholdsvis "Non-linear Least Squares method" og "Capons method", som kan brukes til å beregne fundamentalfrekvensen til harmonisk støy. Vi tilpasser metodene til støyen og evaluerer dem i henhold til treffsikkerhet og beregningstid. Resultatene viser at "Capon" estimatoren utmerker seg på treffsikkerhet ved lav signal til støyforhold, men at det koster; "Non-linear Least Squares" estimatoren bruker en sjettedel av beregningstiden til "Capon" estimatoren. Siden "Non-linear Least Squares" estimatoren utmerker seg i beregningstid er den å foretrekke. Spesielt siden det åpner for å beregne med lengere data segmenter og fortsatt opprettholde forspranget i beregningstid.

Contents

1 Introduction **1**

2 Theory **3**
2.1 Radiated noise . . . 3
2.1.1 Dispersion . . . 4
2.1.2 Waveguide . . . 5
2.1.3 Lloyd's mirror effect . . . 5
2.1.4 Doppler shift . . . 5
2.2 Signal Model . . . 6

3 Method **7**
3.1 Non-linear Least Squares Estimator . . . 7
3.1.1 Derivation of NLS Estimator . . . 7
3.1.2 Implementation . . . 8
3.2 Capon Estimator . . . 9
3.2.1 Derivation of Capon Estimator . . . 9
3.2.2 Implementation . . . 12
3.3 Average line . . . 13
3.4 Frequency tracking . . . 15

4 Analysis of Dataset **17**
4.1 Dataset description . . . 17
4.2 Analysis of data . . . 19
4.2.1 Boat One . . . 19
4.2.2 Boat two . . . 20
4.2.3 Boat three . . . 21
4.2.4 Ambient noise . . . 21

5 Results **25**
5.1 Accuracy at low SNR . . . 25
5.2 Estimator applied to dataset . . . 27
5.2.1 Boat one . . . 27
5.2.2 Boat two . . . 32
5.2.3 Boat three . . . 39

5.2.4 Ambient noise 41
5.3 Summary of results 42

6 Discussion **43**

7 Conclusion **47**

References **49**

A NLS estimator Matlab Implementation **51**

B Capons estimator Matlab Implementation **53**

C Autocorrelation matrix implementation - acorrmat.m **55**

List of Figures

3.1 The number of possible harmonics for each fundamental frequency in ζ. 14
3.2 Normalized cost functions calculated with noise $\sigma^2 = 1$. 15
3.3 Weighted and normalized cost functions from noise with noise $\sigma^2 = 1$, and $span = 0.15$. 16

4.1 Spectrogram of acoustic pressure from passage of boat number 1. 20
4.2 Spectrogram of acoustic pressure from passage of boat number 2. 21
4.3 Spectrogram of acoustic pressure from passage of boat number 3. . 22
4.4 Spectrum of the ambient noise sample. 23

5.1 Estimator hits from applying the estimators to synthetic data of varying SNR. The blue line indicates the hits from the NLS estimator, while the orange line displays that of the Capon estimator. 26
5.2 Spectrum of snapshot 150 from boat 1. 28
5.3 Cost function calculated for boat 1. The blue line represents the cost function, while the orange line is the LOWESS line. 29
5.4 Normalized, weighted cost functions calculated for boat 1. The upper plot shows the cost function for NLS, while the lowermost plot shows Capon. 30
5.5 Harmonic amplitudes of snapshot 150 for boat 1 calculated using equation 3.2. 30
5.6 Tracking of fundamental frequency for boat 1. The blue line illustrates the NLS result, while the orange line indicates that of Capon. 31
5.7 Spectrogram of acoustic pressure radiation captured from boat 1. The magenta and black lines indicate harmonic frequencies estimated by Capon and NLS, respectively. See figure 4.1 for spectrogram. 32
5.8 Spectrum of snapshot 150 from boat 2. 33
5.9 Cost function calculated for boat 2. In the upper sub-plot, we can see the graphs for NLS, while Capons are in the lower sub-plot. The blue line represents the cost function, while the orange line is the LOWESS line. 34

5.10 Normalized, weighted cost functions calculated for boat 2. The upper plot shows the cost function for NLS, while the lowermost plot shows Capon. 35
5.11 Harmonic amplitudes of snapshot 150 for boat 2 calculated using equation 3.2. 36
5.12 Tracking of fundamental frequency for boat 2. The blue line illustrates the NLS result, while the orange line indicates that of Capon. 37
5.13 Spectrogram of acoustic pressure radiation captured from boat 2. The magenta lines indicate harmonic frequencies estimated by Capon and the black lines those of NLS. See figure 4.2 for spectrogram. 38
5.14 Spectrum of snapshot 1050 from boat 3. 39
5.15 Cost function calculated for boat 3. In the upper sub-plot, we can see the graphs for NLS, while Capons are in the lower sub-plot. The blue line represents the cost function, while the orange line is the LOWESS line. 40
5.16 Harmonic amplitudes of snapshot 1050 for boat 3 calculated using equation 3.2. 40
5.17 Cost function calculated for snapshot 150 of the ambient noise. In the upper sub-plot, we can see the graphs for NLS, while Capons are in the lower sub-plot. The blue line represents the cost function, while the orange line is the LOWESS line. 41

List of Tables

2.1 Small boat noise sources. 4

4.1 Description of dataset. 18

5.1 Description of synthetic dataset used in hits against SNR comparison of estimators. 26
5.2 Average computation time for estimators on synthetic noise. 27
5.3 Estimated fundamental frequencies and raw cost function values for boat passages (1-3) and for ambient noise (4). 42

Nomenclature

$a_{k,l}$	Amplitude and phase of the l-th harmonic in the k-th harmonic series
$\boldsymbol{a}$	Vector of amplitude and phase information
$\widehat{\boldsymbol{a}}$	Estimator for amplitude and phase of harmonic signal
$\boldsymbol{C}$	Harmonic amplitude matrix
c_0	Nominal sound speed
CPA	Closest Point of Approach
$\boldsymbol{\Gamma}_0$	Optimal filter used to derive Capon estimator
d	Dampening constant
D	Water depth
$\boldsymbol{E}$	Eigenvalue matrix with eigenvalues of $\boldsymbol{R}$
f_1	Fundamental frequency [Hz]
f_s	Sampling frequency
f_{max}	Maximum search frequency for ζ in Hertz
f_{min}	Minimum search frequency for ζ in Hertz
$\boldsymbol{F}$	Lagrange function
$\boldsymbol{I}$	Identity matrix
J_{NLS}	NLS cost function
J_{Capon}	Capon cost function
K	Number of different fundamental frequencies
L	Number of harmonics in a harmonic series
$\boldsymbol{\lambda}$	Lagrange multiplier
m	Mode number
N	Snapshot length
N_b	Number of blades

$\widehat{\omega_1}$	Estiamted fundamental frequency
ϕ	Phase of a signal
$\boldsymbol{P}$	Capon calculation simplification matrix
$\boldsymbol{R}$	Autocorrelation matrix
RPM	Revolutions Per Minute
$\boldsymbol{V}$	Matrix of eigenvectors of $\boldsymbol{R}$
$\boldsymbol{w}$	Vector of noise
$w(n)$	Additive noise
$x(m)$	Discrete signal
$\widetilde{x}(n)$	Signal snapshot
$\widetilde{\boldsymbol{x}}$	Signal snapshot vector
$\boldsymbol{Z}$	Vandermonde matrix - Signal model
ζ	Range of frequencies to search for the fundamental frequency

Chapter 1

Introduction

The focus of this thesis is to analyse noise radiated from small vessels, such as recreational boats, with emphasis on estimating their harmonic signature, often referred to as pitch estimation. The study is of interest in regards to anthropogenic noise in the marine environment. There has been an increased focus on this within the EU in the recent years. The work in this thesis has a focus on recognizing noise from small boats by detecting their harmonic signature. Not much work appears to have been done in order to classify noise from small vessels. Previous work in the field, such as (Sorensen, Ou, Zurk, & Siderius, 2010) and (Ogden, Zurk, Jones, & Peterson, 2011), have focused on detecting and tracking vessels in Marine Protected Areas, for activity which is not meant to be present in such places. This thesis focuses on applying the estimation methods developed by (Christensen, Stoica, & Jensen, 2007) to underwater acoustic data due to small vessels. The dataset has been collected with the hydrophone sensors on the NILUS (Networked Intelligent Under-water Sensor) nodes developed by FFI.

A lot of work in the field of pitch estimation is performed with speech in mind. Previous work, as (Nehorai & Porat, 1986) and (Wise, Caprio, & Parks, 1976), usually consider either filter based methods or statistical methods similar to the Maximum Likelihood Estimator. Our focus is on the Non-linear Least Squares and Capon estimators presented by (Christensen et al., 2007) and investigated in (Faltin, 2014), applied to noise similar to that introduced by (Ogden et al., 2011), containing both a harmonic noise component, and a broadband noise component.

Chapter 2 introduces the signal model, and relevant acoustic theory used in the thesis. In Chapter 3, we develop our estimators, and comment on aspects that are vital for these kinds of estimators. Chapter 4 presents an analysis of the dataset. We present our results in Chapter 5, and discuss them in Chapter 6. Finally, in Chapter 7, we draw a conclusion from our experience with the estimators.

Chapter 2

Theory

In this chapter we will present relevant acoustic theory for this thesis. We will focus our view on how our dataset originates from the marine environment, and how it is affected from this.

2.1 Radiated noise

Noise from small boats consist of an harmonic and a broadband part. In our application, we will think of the harmonic part of the noise as our signal, and broadband noise as part of the total noise. In addition to the noise from our vessel, we have to assume that there is ambient noise, but we assume this to complement the broadband noise of our vessels. Table 2.1, adapted from (Ogden et al., 2011), lists the ship components and effects which are likely to contribute with harmonic noise and their relationships. The table states that both factors in the engine, like the Revolutions Per Minute (RPM), and the propeller, for example its number of blades (N_b), affect the radiated harmonic noise.

Harmonic noise is defined as a sound composed of a series of sinusoidal tones with frequencies which are integer multiples of a fundamental f_1. We define our signal by

$$s(n) \;=\; \sum_{l=1}^{L} a_l \sin\left(2\pi f_1 l n + \phi(l)\right) \tag{2.1}$$

where n is a time index, and a_l is an (unknown) coefficient. The noise includes L harmonics with frequency $f_1 \cdot l$ and phase $\phi(l)$. In our situation we have to assume the harmonic signal to be distorted by both additive coloured noise and different effects that affect sounds in an ocean environment. The major effects

Table 2.1: Small boat noise sources.

Engine Rates	
Cylinder Firing Rate	$f_{CF} = f_{CR}/2$
Crankshaft Rotation Rate	$f_{CR} = RPM/60$
Engine Speed	RPM
Engine Firing Rate	$f_{EF} = N_c f_{CF}$
Number of Cylinders	N_c
Propeller Rates	
Shift Rotation Rate	$f_{SR} = f_{CR}/\Lambda_g$
Gear Ratio	Λ_g
Blade Rotation Rate	$f_{BR} = N_b f_{SR}$
Number of Blades	N_b

we can expect to affect our data are *dispersion*, *waveguide cutoff*, *Lloyd's mirror effect*, and *Doppler shift*. The received signal on our hydrophone is thus

$$x(n) \;=\; \sum_{l=1}^{L} a_l \sin\left(2\pi f_1 l n + \phi(l)\right) + w(n) \tag{2.2}$$

where $w(n)$ denotes broadband noise consisting of everything in the received signal excluding the harmonic part defined in equation 2.1.

2.1.1 Dispersion

When acoustic waves propagate in water, different parts of the spectrum travels at slightly different speeds. This can result in signal distortion with distance. Thus, the harmonics observed at the hydrophone may be out of sync with each other when the signal is propagating over long ranges (Hovem, 2012, p. 156-157). In our case, this effect is most likely a problem only for very long ranges. (Faltin, 2014, p. 6)

2.1.2 Waveguide

We can consider the marine environment to be an acoustic waveguide; a structure where acoustic waves can propagate. A waveguide can have several modes which define how sound is carried in the medium. For example, an ideal waveguide has an infinitely hard and totally reflecting seabed, and total reflection and a phase shift at the surface. The lowest frequency that can propagate, or cutoff frequency, in such a waveguide is (Hovem, 2012, p. 159-163)

$$f_{0,m} = \frac{c_0}{4D}(2m-1) \tag{2.3}$$

Where D is the sea depth, and c_0 is the nominal sound speed. The mode number, m, defines which mode we are considering. Frequencies below the cutoff frequency of mode 1 will not propagate over longer distances in the waveguide.

2.1.3 Lloyd's mirror effect

The Lloyd's mirror effect is easily spotted in noise from passing ships and is sometimes called *the bathtub effect*. The effect comes from the different arrival times and phase shifts of signals travelling in direct paths from the source to the receiver, and signals that travel in alternative paths. The signal arriving at multiple times with different travel distances makes up for a received signal with multiple phase distortions. These distortions can cancel out the signal at some places in the spectrum, and amplify it in other. This is a range dependant transmission effect, and the effect changes as the source is moving.

2.1.4 Doppler shift

As we are looking at the harmonic frequencies in our signals, which are the noises that boats radiate when they pass by our sensor, we have to expect to see a frequency shift from the Doppler effect; sound received from a source which is moving towards a stationary observer appears to have a higher frequency than what it originally radiated. The opposite happens when the source is moving away from the observer. The effect occurs because of the difference in speed between source and observer.

2.2 Signal Model

The signal used in this thesis are determined by K fundamental frequencies ω_k and an unknown number of harmonics with amplitudes and phases described by $a_{k,l}$. We assume the sampled signal $x(n)$ has a time varying fundamental frequency $\omega(t)$. For simplicity we define $\widetilde{x}(n)$ for $n \in \{0, 1, \cdots, N-1\}$ to be a snapshot of $x(n)$ where we assume ω_k to be stationary. The observed signal is then (Christensen et al., 2007)

$$\widetilde{x}(n) \;=\; \mathbf{Re}\left\{\sum_{k=1}^{K}\left(\sum_{l=1}^{L} a_{k,l}e^{j\omega_k ln}\right)\right\} + w(n) \tag{2.4}$$

where $w(n)$ is additive noise, and $\mathbf{Re}\{\cdot\}$ denotes the real part of a complex number. In this thesis we assume one fundamental frequency, or source, implying $K = 1$. The number of harmonics, L, are assumed unknown.

Our signal snapshot can be expressed as equation (2.6). $\boldsymbol{a}$ represents the amplitude and phase information of the signal. The $\boldsymbol{Z}$ matrix, which is a Vandermonde matrix, represents the frequency information in the signal, and is calculated from

$$\boldsymbol{Z} = \begin{bmatrix} 1 & 1 & \cdots & 1 \\ \exp(j\omega) & \exp(2j\omega) & \cdots & \exp(Lj\omega) \\ \exp(2j\omega) & \exp(4j\omega) & \cdots & \exp(2Lj\omega) \\ \vdots & \vdots & \ddots & \vdots \\ \exp((N-1)j\omega) & \exp(2(N-1)j\omega) & \cdots & \exp(L(N-1)j\omega) \end{bmatrix} \tag{2.5}$$

We define $\boldsymbol{w}$ to be the vector of noise. We can then express the signal snapshot

$$\widetilde{\boldsymbol{x}} \;=\; \boldsymbol{Z}\boldsymbol{a} + \boldsymbol{w} \tag{2.6}$$

We define ζ to be the range of angular frequencies where we expect the fundamental frequency to be located. The $\boldsymbol{Z}$ matrix is calculated for every frequency ω in ζ. The objective for our estimator is then to find the best estimate for $\widehat{\omega_1}$ within ζ, for a given snapshot of data, $\widetilde{\boldsymbol{x}}$.

Chapter 3

Method

In this chapter we will present the signal processing methods used in this thesis work. These methods are the Non-linear Least Squares and Capon Methods. Both of these methods are based on the signal model presented in section 2.2.

3.1 Non-linear Least Squares Estimator

3.1.1 Derivation of NLS Estimator

The derivation of the NLS estimator is from (Faltin, 2014).

We want to find an expression for $\widehat{\omega_1}$, the estimated fundamental frequency of the harmonic part of the N length column vector $\boldsymbol{x}$. We assume that $\omega_1 \in \zeta$. The Vandermonde matrix $\boldsymbol{Z}$ is a function of ζ. In this derivation we assume $\boldsymbol{Z} \in \mathbb{C}^{N \times L}$, and that $\boldsymbol{I}$ is the $L \times L$ identity matrix. The definition of the Non-linear Least Squares problem is

$$\widehat{\omega_1} \quad = \quad \arg\min_{\zeta} \|\boldsymbol{x} - \boldsymbol{Z}\,\boldsymbol{a}\|_2^2 \tag{3.1}$$

Where $\|\cdot\|_2$ denotes the L^2 norm. To minimize this expression, we minimize the error $\boldsymbol{\epsilon} = \boldsymbol{x} - \boldsymbol{Z}\boldsymbol{a}$, by setting it equal to $\boldsymbol{0}$, which implies (Aster, Borchers, & Thurber, 2011)

$$\boldsymbol{Z}\boldsymbol{a} \quad = \quad \boldsymbol{x} \tag{3.2}$$

Since $\boldsymbol{Z}$ is in general not invertible, we have to multiply by $\boldsymbol{Z}^{\boldsymbol{H}}$ on both sides in order to make $\boldsymbol{a}$ separable. By doing this, as well as multiplying by the inverse

matrix of $\boldsymbol{Z^H}\ \boldsymbol{Z}$ we end up with equation (3.3), expressing $\widehat{\boldsymbol{a}}$ in terms of $\boldsymbol{Z}$ and $\boldsymbol{x}$. $(\cdot)^H$ denotes the Hermitian, or the complex transpose.

$$\widehat{\boldsymbol{a}} \quad = \quad (\boldsymbol{Z}^H\,\boldsymbol{Z})^{-1}\,\boldsymbol{Z}^H\,\boldsymbol{x} \tag{3.3}$$

This equation can be used to estimate the harmonic amplitudes once the fundamental frequency is known. By inserting equation (3.3) into equation (3.1) we get

$$\widehat{\omega_1} \quad = \quad \arg\min_{\zeta} \|\boldsymbol{x} - \boldsymbol{Z}(\boldsymbol{Z}^H\boldsymbol{Z})^{-1}\boldsymbol{Z}^H\boldsymbol{x}\|_2^2 \tag{3.4}$$

This expression can be simplified by multiplying with $\boldsymbol{x^H}$ inside the norm.

$$\widehat{\omega_1} \quad = \quad \arg\min_{\zeta} \|\boldsymbol{x}^H\boldsymbol{x} - \boldsymbol{x}^H\boldsymbol{Z}(\boldsymbol{Z}^H\boldsymbol{Z})^{-1}\boldsymbol{Z}^H\boldsymbol{x}\|_2^2 \tag{3.5}$$

The first expression in the norm of equation (3.5) only depends on $\boldsymbol{x}$, meaning that it is dependant of ζ. Instead of minimizing the difference of the two terms, we can therefore maximize the second term. (Christensen et al., 2007; Kay, 1993)

$$\widehat{\omega_1} \quad = \quad \arg\max_{\zeta} \boldsymbol{x}^H\boldsymbol{Z}(\boldsymbol{Z}^H\boldsymbol{Z})^{-1}\boldsymbol{Z}^H\boldsymbol{x} \tag{3.6}$$

It is this equation we can use to perform the estimation. An interesting thing though, is that $\boldsymbol{Z}^H\boldsymbol{Z}$ approaches $N \cdot \boldsymbol{I}$ as N becomes large (Christensen et al., 2007). We can therefore skip this inverse part of the estimator. Thus, the estimator can be expressed

$$\widehat{\omega_1} \quad = \quad \arg\max_{\zeta} \boldsymbol{x}^H\boldsymbol{Z}\boldsymbol{Z}^H\boldsymbol{x} \tag{3.7}$$

If we had used a weighted signal model as suggested in (Faltin, 2014), we would have to use equation 3.6 in order to get a correct equation.

3.1.2 Implementation

Our implementation of the NLS estimator is dependant on having the following variables pre determined.

1. $x[n]$ - signal snapshot vector
2. N - snapshot length
3. ζ - vector of angular frequencies in which to search for the fundamental frequency
4. L - number of harmonics
5. spann - LOWESS span parameter

In our implementation we have assumed that L is unknown. What we do to make this transparent in these works is to calculate the maximum number of harmonics that can fit inside the Nyquist frequency of $f_s/2$ for each frequency in ζ.

When these variables are known, we generate a Vandermonde matrix $\boldsymbol{Z}$ from equation 2.5 for each frequency in ζ. We can then calculate equation 3.6, and put the value in our cost function, $J_{NLS}(\zeta)$. When the cost function is calculated for every ζ value, we can find our estimate; $\widehat{\omega_1}$ is the frequency in ζ which corresponds to the largest value for our cost function, $J_{NLS}(\zeta)$. The implementation of the NLS estimator which is used in this thesis can be found in appendix A

3.2 Capon Estimator

3.2.1 Derivation of Capon Estimator

The derivation of the Capon estimator is from (Faltin, 2014).

The Capon estimator derivation is based on finding the L filters in $\boldsymbol{\Gamma}$ that pass all the power at specific frequencies. In this derivation we define the autocorrelation matrix $\boldsymbol{R} = E\{\boldsymbol{x}\boldsymbol{x}^H\} \in \mathbb{C}^{N\times N}$, the Vandermonde matrix $\boldsymbol{Z} \in \mathbb{C}^{N\times L}$, the harmonic amplitude matrix $\boldsymbol{C} \in \mathbb{C}^{L\times L}$, the set of filters which define the method $\boldsymbol{\Gamma} \in \mathbb{C}^{L\times N}$, and $\boldsymbol{I}$ is the $L \times L$ identity matrix. To generalize we define $\boldsymbol{C} = \boldsymbol{I}$, meaning that we assume unitary harmonic amplitudes. This filter design problem is defined by the statement (Christensen et al., 2007; Stoica & Moses, 2005)

$$\min_{\Gamma} \ \mathrm{Tr}\left[\boldsymbol{\Gamma}^H \boldsymbol{R}\boldsymbol{\Gamma}\right] \text{ subject to } \boldsymbol{\Gamma}^H\boldsymbol{Z} = \boldsymbol{C} \tag{3.8}$$

where $\mathrm{Tr}[\cdot]$ denotes the trace operator. Equation (3.8) is solved using Lagrange multipliers. We want to minimize $f(\boldsymbol{\Gamma}) = \boldsymbol{\Gamma}^H\boldsymbol{R}\boldsymbol{\Gamma}$ with the constraint $g(\boldsymbol{\Gamma}) =$

$\boldsymbol{\Gamma}^H \boldsymbol{Z} - \boldsymbol{C}$. We define

$$\boldsymbol{F}(\boldsymbol{\Gamma}, \lambda) \;=\; f(\boldsymbol{\Gamma}) - \lambda g(\boldsymbol{\Gamma}) = \boldsymbol{\Gamma}^H \boldsymbol{R} \boldsymbol{\Gamma} - \lambda(\boldsymbol{\Gamma}^H \boldsymbol{Z} - \boldsymbol{C}) \tag{3.9}$$

to be the Lagrange function. The method of Lagrange multipliers involves minimizing the partial derivatives of $\boldsymbol{F}$, where f is the function we want to minimize, g is the constraint, and λ is the Lagrange multiplier. This introduces equations (Petersen & Pedersen, 2012)

$$\frac{\partial \boldsymbol{F}(\boldsymbol{\Gamma}, \lambda)}{\partial \boldsymbol{\Gamma}} \;=\; (\boldsymbol{R}^H + \boldsymbol{R})\, \boldsymbol{\Gamma} - \lambda \boldsymbol{Z} = \boldsymbol{0} \tag{3.10}$$

$$\frac{\partial \boldsymbol{F}(\boldsymbol{\Gamma}, \lambda)}{\partial \boldsymbol{\lambda}} \;=\; \boldsymbol{\Gamma}^H \boldsymbol{Z} \;-\; \boldsymbol{C} \;=\; \boldsymbol{0} \tag{3.11}$$

Now we have two unknowns in (3.10), and we need to reduce this number to one. Looking at equation (3.11) we can see that this yields the exact same statement as the constraint in equation (3.8). Also, by definition, since $\boldsymbol{R}$ is hermitian $\boldsymbol{R} + \boldsymbol{R}^H = 2\boldsymbol{R}$

$$\boldsymbol{\Gamma}^H \boldsymbol{Z} \;=\; \boldsymbol{C} \tag{3.12}$$

Note that this is the same as

$$\boldsymbol{Z}^H \boldsymbol{\Gamma} \;=\; \boldsymbol{C}^H \tag{3.13}$$

Now, we start to reformulate (3.10) to find an expression for λ. Multiplying by the inverse of $2\boldsymbol{R}$ leads to

$$\boldsymbol{\Gamma} \;=\; \lambda (2\boldsymbol{R})^{-1} \boldsymbol{Z} \tag{3.14}$$

By realizing that we can enforce the left side of equation (3.14) to become $\boldsymbol{C}^H = \boldsymbol{Z}^H \boldsymbol{\Gamma}$ by multiplying with $\boldsymbol{Z}^H$ we can introduce the constraint. Thus we have utilized two equations, and we can get solutions for the two variables

$$\boldsymbol{C}^H \;=\; \lambda \boldsymbol{Z}^H (2\boldsymbol{R})^{-1} \boldsymbol{Z} \tag{3.15}$$

Now, we simply separate λ from the matrices and obtain

$$\boldsymbol{\lambda} \;=\; (\boldsymbol{Z}^H(2\boldsymbol{R})^{-1}\boldsymbol{Z})^{-1}\boldsymbol{C}^H \tag{3.16}$$

Inserting equation (3.16) into equation (3.10) gives

$$(2\boldsymbol{R})\,\boldsymbol{\Gamma} = \; 2\,\boldsymbol{Z}(\boldsymbol{Z}^H(\boldsymbol{R})^{-1}\boldsymbol{Z})^{-1}\boldsymbol{C}^H \tag{3.17}$$

We multiply with the inverse of $\boldsymbol{R}$ to get an expression for the minimizing $\boldsymbol{\Gamma}_0$

$$\boldsymbol{\Gamma}_0 \;=\; (\boldsymbol{R})^{-1}\boldsymbol{Z}(\boldsymbol{Z}^H(\boldsymbol{R})^{-1}\boldsymbol{Z})^{-1}\boldsymbol{C}^H \tag{3.18}$$

We now have the minimizing $\boldsymbol{\Gamma}_0$, and we can go further towards finding an expression for the optimal Capon estimator. We start by inserting the optimal $\boldsymbol{\Gamma}_0$ into the the function which we minimized. Though, we need to find $\boldsymbol{\Gamma}_0^H$ first.

$$\boldsymbol{\Gamma}_0^H \;=\; \boldsymbol{C}\,((\boldsymbol{Z}^H(\boldsymbol{R})^{-1}\boldsymbol{Z})^H)^{-1}\boldsymbol{Z}^H((\boldsymbol{R})^{-1})^H \tag{3.19}$$

Inserting the expressions for $\boldsymbol{\Gamma}_0$ and $\boldsymbol{\Gamma}_0^H$ into $\boldsymbol{\Gamma}^H\boldsymbol{R}\boldsymbol{\Gamma}$

$$\boldsymbol{\Gamma}_0^H\boldsymbol{R}\boldsymbol{\Gamma}_0 \;=\; \boldsymbol{C}\,((\boldsymbol{Z}^H\boldsymbol{R}^{-1}\boldsymbol{Z})^H)^{-1}\boldsymbol{Z}^H(\boldsymbol{R}^{-1})^H\boldsymbol{R}\boldsymbol{R}^{-1}\boldsymbol{Z}(\boldsymbol{Z}^H\boldsymbol{R}^{-1}\boldsymbol{Z})^{-1}\boldsymbol{C}^H \tag{3.20}$$

Reducing this by recognizing that $\boldsymbol{R}\boldsymbol{R}^{-1} = \boldsymbol{I}$ and that $\boldsymbol{Z}^H(\boldsymbol{R}^{-1})^H\boldsymbol{Z} = (\boldsymbol{Z}^H\boldsymbol{R}^{-\mathbf{1}}\boldsymbol{Z})^H$ gives us this equation

$$\boldsymbol{\Gamma}_0^H\boldsymbol{R}\boldsymbol{\Gamma}_0 \;=\; \boldsymbol{C}\,(\boldsymbol{Z}^H\boldsymbol{R}^{-\mathbf{1}}\boldsymbol{Z})^{-1}\boldsymbol{C}^H \tag{3.21}$$

This is the minimized output of the filter that passes the power at L harmonic frequencies defined in equation (3.8). Though, this is not exactly what we want. We are searching for a set of filters which pass the maximum amount of power in specific frequencies. This can be done by searching for the argument of the maximum of the trace defined by inserting 3.21 into 3.8

$$\widehat{\omega_1} \;=\; \arg\max_{\zeta}\;\mathrm{Tr}\left[\boldsymbol{C}\,\left(\boldsymbol{Z}^H\boldsymbol{R}^{-1}\boldsymbol{Z}\right)^{-1}\boldsymbol{C}^H\right] \tag{3.22}$$

If $\boldsymbol{x}$ is real, meaning that $\boldsymbol{R}$ is symmetric, we could simplify further using eigenvalue decomposition as in (Christensen et al., 2007). To do this, we define $\boldsymbol{V}$ and $\boldsymbol{E}$ to be the matrices of eigenvectors and eigenvalues of $\boldsymbol{R}$ such that $\boldsymbol{R} = \boldsymbol{V}\boldsymbol{E}\boldsymbol{V}^{-1}$. We insert $\boldsymbol{C} = \boldsymbol{I}$, implying unitary harmonics amplitudes. The estimator can be expressed

$$\widehat{\omega_1} \;=\; \arg\max_{\zeta} \;\mathrm{Tr}\left[\left(\boldsymbol{Z}^H\boldsymbol{V}\boldsymbol{E}^{-1/2}\left(\boldsymbol{Z}^H\boldsymbol{V}\boldsymbol{E}^{-1/2}\right)^H\right)^{-1}\right] \tag{3.23}$$

Unlike the NLS estimator, the Capon estimator does not give an estimator for the harmonic amplitude and phase information. For an estimate of the amplitude and phase of the harmonics we will use equation 3.2.

3.2.2 Implementation

Like the NLS estimator, the Capon estimator needs a number of values and vectors before calculations start. These values and vectors are the same as the NLS needed. However, the Capon estimator, equation 3.23, has some aspects which make it more difficult to implement; the equation includes two matrix inversions. These are known to be calculation inefficient. The inner inversion was solved by applying an eigenvalue decomposition, which means that we can get through the first inversion with the inversion of a diagonal matrix. The second inversion is harder to implement, and a Singular Value Decomposition is favourable. In this implementation, we use the *pinv.m* function which is built into Matlab.

When these factors are known, we start by estimating our sample autocorrelation or autocovariance matrices. In appendix C a simple Matlab implementation of an autocorrelation matrix function is listed. After applying the *eig.m* function to get the eigenvalues, $\boldsymbol{E}$, and eigenvectors, $\boldsymbol{V}$, we calculate the product $\boldsymbol{P} = \boldsymbol{V}\boldsymbol{E}^{-1/2}$. By doing this we have calculated all the frequency independent factors, and we are left with two instances of the $\boldsymbol{Z}$ matrix multiplied by $\boldsymbol{P}$

$$\widehat{\omega_1} \;=\; \arg\max_{\zeta} \;\mathrm{Tr}\left[\left(\boldsymbol{Z}^H\boldsymbol{P}\left(\boldsymbol{Z}^H\boldsymbol{P}\right)^H\right)^{-1}\right] \tag{3.24}$$

When the product is calculated, we can take the trace of its inverse. Searching for the estimated fundamental is done by finding the ζ value which corresponds

to the maximum of the estimators output. The Capon estimator implementation can be found in appendix B.

Due to the Capon product, $\boldsymbol{Z}^H\boldsymbol{P}\left(\boldsymbol{Z}^H\boldsymbol{P}\right)^H$, being reported close to singular for small values of ζ by the *cond.m* function in Matlab, we cannot search in extremely low frequencies. Therefore, we set a lowest possible ζ value equivalent to 10 Hz. This workaround does solve the problem for snapshot lengths larger then a tenth of the numerical value of the sampling frequency with our dataset.

3.3 Average line

For our dataset we have to expect that there are a number of harmonics in the signal equal to the maximum possible for any given fundamental frequency to ensure that the methods take key components into account.

Since we operate with an unknown number of harmonics, and expect them to reside in the entire spectrum, we have to assure that the number of harmonics we assume to be present for each frequency in ζ is the maximum of what is possible. Because of this, we calculate the number of harmonics for a given frequency after equation 3.25. Though, for very low frequencies we have set a limit. In our applications, we set a maximum harmonic length, $\max(L) = 100$. We can calculate the number of harmonics for the resulting possible fundamental frequencies in ζ by

$$L(\zeta) = \frac{f_s/2}{\zeta} \tag{3.25}$$

The numbers in the resulting vector $\boldsymbol{L}$ is rounded downwards to the closest integer. Calculating equation 3.25 with $f_s = 3000$ Hz and $\zeta \in [10, 65]$ gives the plot in figure 3.1. This interval is used for ζ throughout the thesis, and is chosen because it both handles the issues we encountered with the Capon product being close to singular below 10 Hz, and also make sure that we search at $2f_1$ in all data samples, where f_1 is the fundamental frequency in Hz.

This variable number of harmonics is necessary for our estimators as we assume an unknown number of harmonics. If we guess too few harmonics we may lose important signature harmonics. On the other hand, if we choose too many harmonics, the estimators find multiple matches at the same frequencies, as should be expected as we can think of them as cyclic FFTs; too many harmonics, and we go multiple times through the spectrum. The result of having a variable number

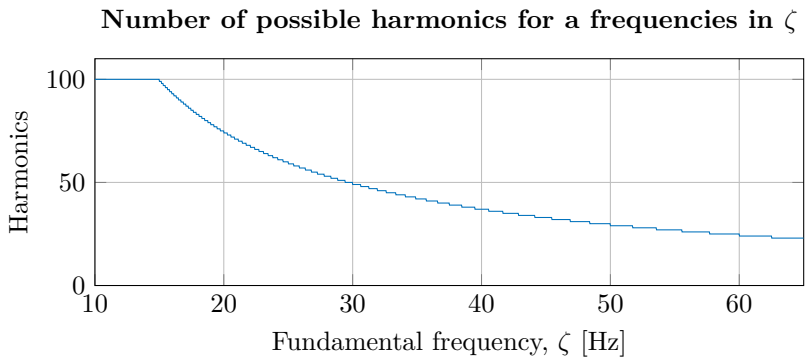

Figure 3.1: The number of possible harmonics for each fundamental frequency in ζ.

of harmonics is that the estimators can result in higher cost functions in lower frequencies than at higher frequencies, as we can see in figure 3.2. In this figure, the cost functions are calculated from white noise with $\sigma^2 = 1$ sampled at 3000 Hz.

From looking at figures 3.1 and 3.2, we can see that the averages of the cost functions appear to be correlated with the number of harmonics. Therefore, we have to do some modifications to get a good enough estimate for certain SNRs. In (Faltin, 2014) we proposed using a weighted cost function to solve a similar problem when we assumed that the harmonic amplitudes decrease with the inverse exponential function such that each harmonic has a lower amplitude than the previous one. This is not a good approach for the NILUS dataset; the signal is filtered with a filter that helps against the decreasing frequency content of the harmonics. In this thesis, we instead propose that we can look at the cost functions with an average line subtracted.

An apparent alternative would be not to decimate the signal, but this would imply that the sample length would have to be increased. With a f_s of 9000 Hz, and a f_{min} of 10 Hz, we would need a snapshot length of at least 900. Not just to get a good resolution, but also to ensure that the Capon inverses would not involve singular matrices. Since we do not correct the filtering in the hydrophone sensor, we have a considerably higher frequency content below 2 kHz than above. This means that fundamental frequencies including more harmonics below 2100 Hz would report a higher cost function than those above. Further, the number of harmonics would have to be set to the least possible, setting an upper limit at $L = f_s/(2f_{max})$, where f_{max} is the largest fundamental we guess. With a f_{max}

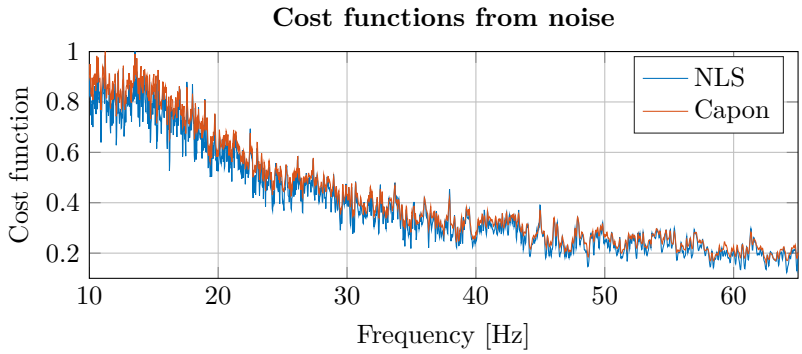

Figure 3.2: Normalized cost functions calculated with noise $\sigma^2 = 1$.

of 65 Hz, this limits us to 69 harmonics, implying that calculating with a ω of 20 would limit us to searching under 1400 Hz.

A way to implement the average line filter in Matlab is by using the built in *smooth.m* function. This function includes a number of implementations that are relevant for our use. These are the moving average and the Locally Weighted Scatterplot Smoothing with both first (LOWESS) and second (LOESS) degree polynomials. By using the local regression it appears that Matlab can find a good fit for the average line of the cost functions. The *smooth.m* function has an optional limitation parameter, *span*, which defines the percentage of the total data to considerer when calculating the regression for each point. Throughout the thesis work, we used a *span* of 0.15 as multiple trials with different values indicated that *span* values in this region gave the best results.

Figure 3.3 shows the cost functions calculated from white noise after LOWESS lines have been subtracted. Here, we can see that the new, weighted cost functions look more like what we should expect when applying the estimators to white Gaussian noise.

3.4 Frequency tracking

Frequency tracking is a vital part of an implementation of these kinds of estimators. In this thesis frequency tracking is done by plotting the estimated fundamental frequency against snapshot number. This is fine for testing, but in a real implementation one could use a logical filter to decide whether there is a

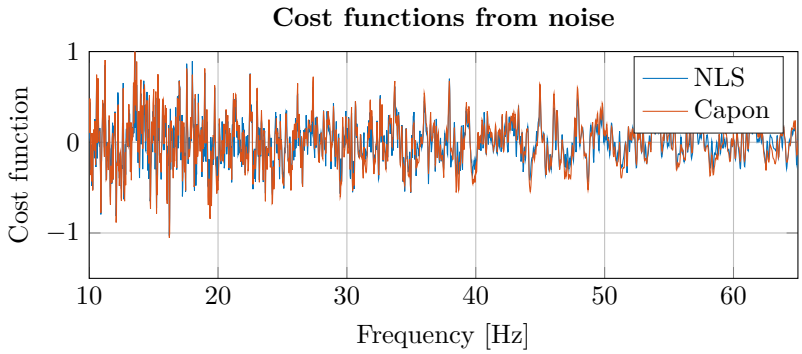

Figure 3.3: Weighted and normalized cost functions from noise with noise $\sigma^2 = 1$, and $span = 0.15$.

frequency track or not. What we propose is a filter which defines a neighbourhood of fundamental frequencies, and if a large majority of this neighbourhood has frequencies which are very similar we can assume all the snapshots to have this fundamental. We could also check whether some snapshots had an estimated fundamental with frequency equal $f_1/2$, $3f_1/2$, or $2f_1$, as these are the most likely misses in a snapshot with a signal of fundamental f_1.

By applying such a filter, we can rectify faulty estimates from sudden sounds in the spectrum. As long as we restrict it properly, by for example, requiring 8 out of 10 fundamentals to hit the same fundamental, we could justify rectifying non-consecutive estimated fundamentals of frequencies equal to those relations described above.

Chapter 4

Analysis of Dataset

4.1 Dataset description

The dataset used to evaluate the methods presented in this thesis were recorded in the waters outside *Vealøs* near *Horten* in the period June 24-26 2014 as part of the "Vealøs 2014" dataset (Smistad, Buen, & Tollefsen, 2014). The hydrophone sensor, which is the sensor used to capture the acoustical pressure variations in water, is attached to the NILUS underwater sensor node. The waters near *Vealøs* are shallow, meaning that the data are influenced by an environment resembling a waveguide. The NILUS node, and thus the hydrophone sensor, is at a depth of 15,5 meters during these measurements.

The three examples used in this thesis are recorded June 24., between 14:00 UTC+2 and 17.15 UTC+2, while there was heavy traffic in the waters outside *Vealøs*. The three boat passings are chosen because they are documented to be of single boats, and since we know which type of boat they are. In addition, we have included an out-take from the *Vealøs 2014* dataset without any immediately apparent boat noise. Table 4.1 lists the types of noise sources in the four data samples of our dataset, and information such as boat length and speed, as well as information about their CPA, or Closest Point of Approach, which is the point in the boat trajectory that is closest to the observer. The boat speeds are estimated from boat position data measured with a *TruPulse* 360^oR *Professional Laser Rangefinder* which is interpolated to estimate the boats trajectory. The CPA time and range of the passages are calculated from the closest point in this trajectory to the known position of the NILUS node. (Smistad et al., 2014)

Table 4.1: Description of dataset.

Number	Type	CPA time [UTC+2]	Boat length [m]	Boat speed [m/s]	CPA range [m]
1	Cabin cruiser	16.36.29	5.49	13.42	71.74
2	Cabin cruiser	17.14.25	6.10	21.18	294.65
3	Sailboat	14.34.34	6.10	2.95	193.98
4	Ambient noise	04.45.23	N/A	N/A	N/A

4.2 Analysis of data

We consider the quality of the three boat passages which the dataset consists of using spectrograms, in a addition to that of the ambient noise using a spectrum. The original sampling frequency in the dataset is 9 kHz. The data segments are all decimated by a factor of three to decrease computation time for the estimation methods, and limit the frequency content. By decimating the signal, in practice we reduce the number of samples by three, as well as reduce the sampling frequency to 3 kHz. This can be done since the hydrophone sensors transfer function strongly dampens most signals over 2 kHz. The usable frequency range for data from this sensor is in the range 10 Hz to 2 kHz, with a known frequency response in between.

For all the spectrograms presented we can see that frequencies below 100 Hz are damped to a high degree, and the lower harmonics are difficult to see without zooming. This effect is likely due to the water outside *Vealøs* being shallow with the depth of 15.5 meters. The approximate cut-off frequency of the first mode is calculated using equation 2.3, assuming an ideal waveguide and a nominal sound speed in water of 1500 meters per second to

$$f_{0,1} \approx \frac{1500\ m/s}{4 \cdot 15.5\ m} \approx 24.2\ \text{Hz} \tag{4.1}$$

The largest issues with noise in our dataset are broadband noise effects such as the Lloyd's mirror effect, and the waveguide cutoff frequency.

4.2.1 Boat One

The first boat passage in the dataset has an approximate CPA distance of 71 meters. The spectrogram of this boat passage, figure 4.1, shows clear harmonic lines in the region between 70 and 950 Hz. We can also notice the CPA time of 1 minute and 18 seconds from both the Doppler frequency shift, and the Lloyd's Mirror interference effects. Some of the harmonics in the lower parts of the spectrum disappear in the broadband noise around the CPA, and a few of the higher harmonics disappear in the Lloyd's mirror effects. This is especially the case for harmonics after CPA.

There are some fluctuation in the harmonic frequencies around 1 minute and 40 seconds. This fluctuation is likely due to a change in propeller RPM, which in turn changes the fundamental frequency. We can also see that a considerable

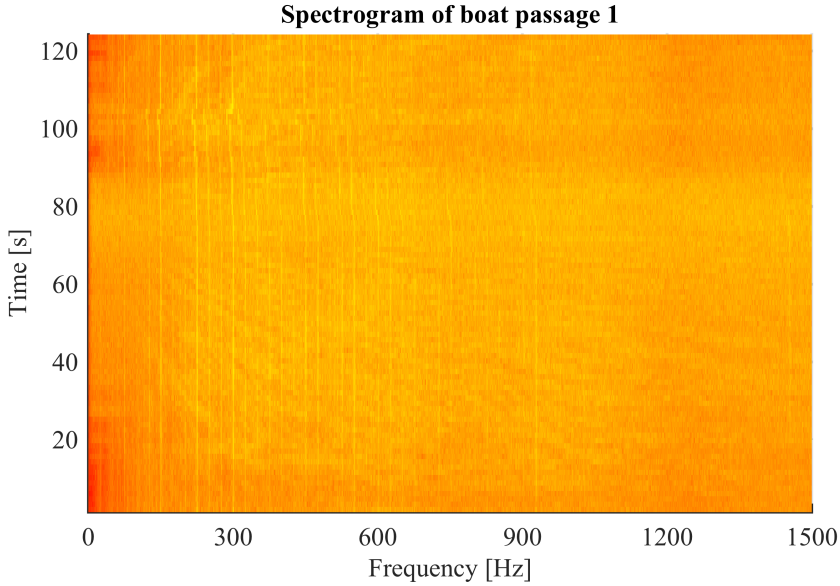

Figure 4.1: Spectrogram of acoustic pressure from passage of boat number 1.

amount of the higher harmonics get hidden by broadband noise around these frequency fluctuations.

4.2.2 Boat two

The noise captured from the second boat appears somewhat cleaner than that of the first boat; in the spectrogram, figure 4.1, we can see that the harmonics do not get hidden by the Lloyd's mirror effect to the same degree as for the first boat, and around 120 seconds we can see clear signs of the harmonics disappearing in the background noise after the passage. the CPA time is easily noticed around the 70 seconds mark by the mentioned Lloyd's mirror effect. The other effect which has to be noted in this spectrogram is that in the areas between 40 and 80 seconds with noticeable low frequency noise; this is likely due to clipping in the recording.

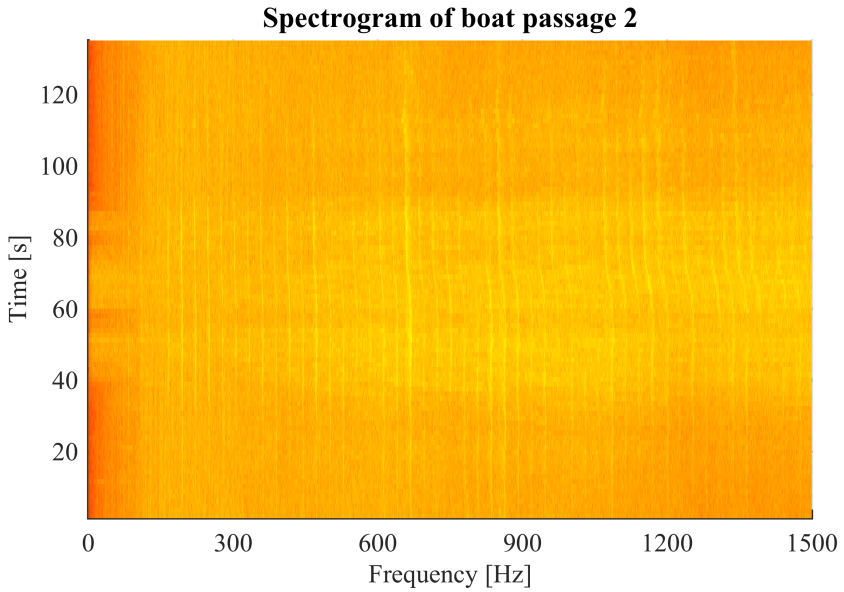

Figure 4.2: Spectrogram of acoustic pressure from passage of boat number 2.

4.2.3 Boat three

Noise recorded from the third boat passage show one property which is present for the passages of boats 1 and 2. As we can see in the spectrogram in figure 4.3, there is a large amount of broadband noise in the frequency band between 400 and 900 Hz. We can also see some additional noise in the region around 150 Hz a while before CPA and some time after. The broadband noise appears to be part of the Lloyd's mirror effect, and we can see a clear bathtub effect with a CPA time around the 150 seconds marker. The fact that the noise has a Lloyd's mirror effect ensures that it is coming from some kind of vessel, and the logbook shows that there is only one boat present at the time; a 6.1 meters long sailboat.

4.2.4 Ambient noise

The last sample from the *Vealøs 2014* dataset we are presenting in this thesis is a typical data segment with no passages done early in the morning, at 04.44 UTC+2 on June 25. In the spectrum of the data sample in figure 4.4, there are

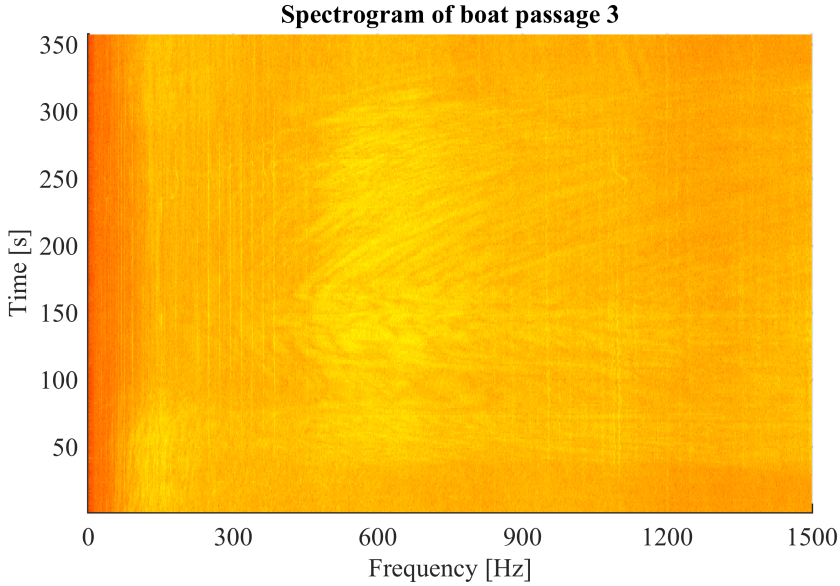

Figure 4.3: Spectrogram of acoustic pressure from passage of boat number 3.

some harmonic frequencies in the region 100 - 300 Hz and one apparently strong frequency component at 757 Hz. These harmonics probably originate from a large ship passage far out at sea, explaining the low SNR. Further, in the spectrum we can see that the power of the noise is increasing in frequencies below 1 kHz and decreasing in frequencies above. We can also see that the noise in the frequency region between 500 and 1200 Hz has power equivalent to the harmonics between 100 and 300 Hz.

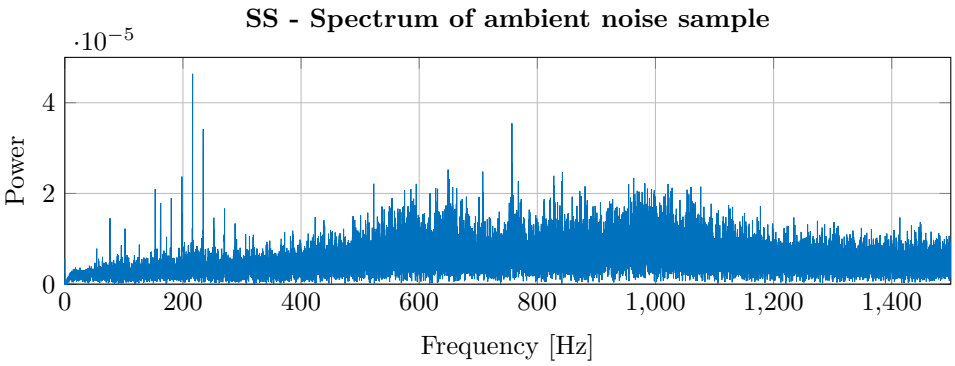

Figure 4.4: Spectrum of the ambient noise sample.

Chapter 5

Results

5.1 Accuracy at low SNR

In (Faltin, 2014, p. 16-20), we investigated how the estimators performed with variable SNR by applying them to synthetic data with different SNR values, and plot the number of estimation hits against SNR. We define a hit as the case that the estimated fundamental is within an interval of 0.4 Hz centred around the actual fundamental. We recalculate the simulations with the new weighting presented in 3.3. The data used to generate the signals used in this plot is listed in table 5.1. The dampening, d, is applied to the amplitude of the harmonics after equation 5.1

$$a_l \;=\; \exp\left(-d(l-1)/L\right), \quad l \in \{1, \cdots, L\} \tag{5.1}$$

Unlike in (Faltin, 2014, p. 16-20), where we did simulations for snapshots of length $N = \{420, 630, 840\}$ samples, we have only calculated using $N = 500$ in these works. This is a considerably shorter snapshot length than the previous calculations, comprising of 1/6 of a second, against 1/5 for the shortest snapshots in the original calculations. However, results presented in figure 5.1 indicate that the weighted algorithm outperform those in the original, where the hit percentage at 0 dB was 80 and 97 for the NLS and Capon estimators, respectively. Results from the new weighting show that both estimators get a hit percentage of 100 at 0 dB. It has to be mentioned that the result from the unweighted calculations achieved a 0 percent hit rate at 6.5 dB SNR for both methods.

From figure 5.1 we can see that the Capon estimator has a slightly higher performance than the NLS estimator at low SNR, though, the computation time is also considerably higher. Table 5.2 lists the average computation time for each method including the subtraction of the LOWESS line. Computation is done

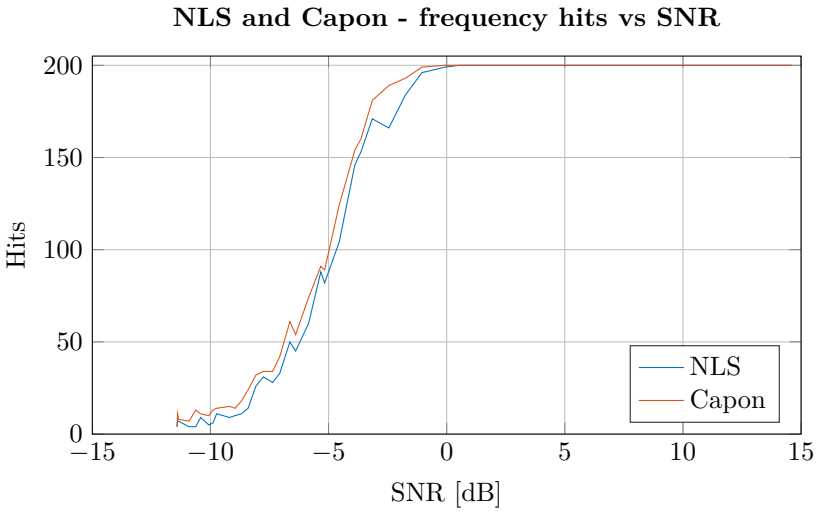

Figure 5.1: Estimator hits from applying the estimators to synthetic data of varying SNR. The blue line indicates the hits from the NLS estimator, while the orange line displays that of the Capon estimator.

Table 5.1: Description of synthetic dataset used in hits against SNR comparison of estimators.

f_1	f_s	L	d	N	σ^2_{min}	σ^2_{max}
26.3783	3000	65	1	500	1^2	20^2

Table 5.2: Average computation time for estimators on synthetic noise.

$\bar{T}_{NLS}$ [s]	$\bar{T}_{Capon}$ [s]
5.71	34.95

inside a *parfor* loop on a currently fast CPU [1]. This table clearly shows that the NLS estimator is almost an order of magnitude faster to calculate at this snapshot length.

5.2 Estimator applied to dataset

In this section the results from the estimators applied to data measured during *Vealøs 2014* are presented. The data presented in this are decimated by 3, and divided into snapshots of 500 samples.

5.2.1 Boat one

To investigate the results of our estimators on the data from boat 1, we will look into snapshot 150 where the fundamental estimates are successful with both methods. Figure 5.2 shows the spectrum using the FFT of the snapshot. The spectrum shows how there is little power in the frequencies below 200 Hz compared to the frequencies above; the lower frequencies are strongly suppressed because of the transfer function of the hydrophone sensor, and the waveguide cutoff.

The top and bottom sub-plots in figure 5.3 display the raw cost functions and LOWESS lines of NLS and Capon, respectively. Apart from the function values, the cost functions appear very similar. The only apparent difference is how the NLS cost function has a slightly higher dynamic range than that of Capon. Notice how the NLS cost function has values in the range 0 - 5000, while Capon has a range of 0 - 25. We can also see a local maximum at the true fundamental in both figures. There is one problem though; the peak at the true fundamental is not the global maximum of the graph. This is due to how the calculations are

[1] Intel Core i7 4790k

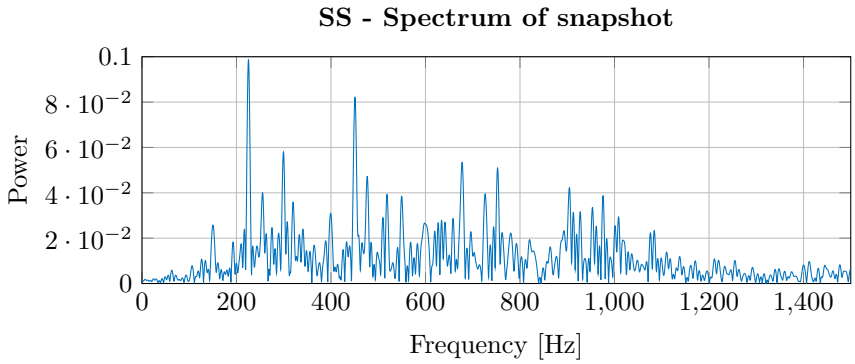

Figure 5.2: Spectrum of snapshot 150 from boat 1.

applied to the dataset. From this knowledge, we can improve the cost function by subtracting the LOWESS line introduced in section 3.3.

By normalizing the result from subtracting the LOWESS lines from their respecting cost functions we get the new cost functions displayed in figure 5.4. In these plots we can see that there is one frequency with a clearly higher cost function than the rest. The frequency location of this peak is our estimate for the fundamental frequency, $f_1 = 25.081$ Hz in this case. In the spectrum of the snapshot, figure 5.2, we can see a high peak around 222 Hz, which corresponds with the estimated harmonic series as the ninth harmonic.

Further, we can use the approximation done when deriving NLS to extract the harmonic amplitudes of the estimated signal. By inserting the estimated fundamental into equation 3.2 we get figure 5.5. This figure has some striking similarities with the spectrum in figure 5.2.

Now, to see how the estimators perform, we introduce figures 5.6 and 5.7. Figure 5.6 shows the tracking of estimated fundamental frequency of the first boat. From figure 5.6 we can see that the fundamental estimate is mostly stable, but has some issues at different places. For example, there is a change in fundamental after snapshot 450, indicating that the CPA is around this time. We can also see that the estimator has some problems with finding a correct fundamental in this region, but this is likely due to broadband noise, as we will investigate further. Recall how we could see that the fundamental changed irregularly 1 minute and 40 seconds out in the file from the spectrogram in figure 4.1. The frequency track also shows some changes in the fundamental around snapshots 545 and 595. These changes in the fundamental frequency corresponds well with the fluctuations in

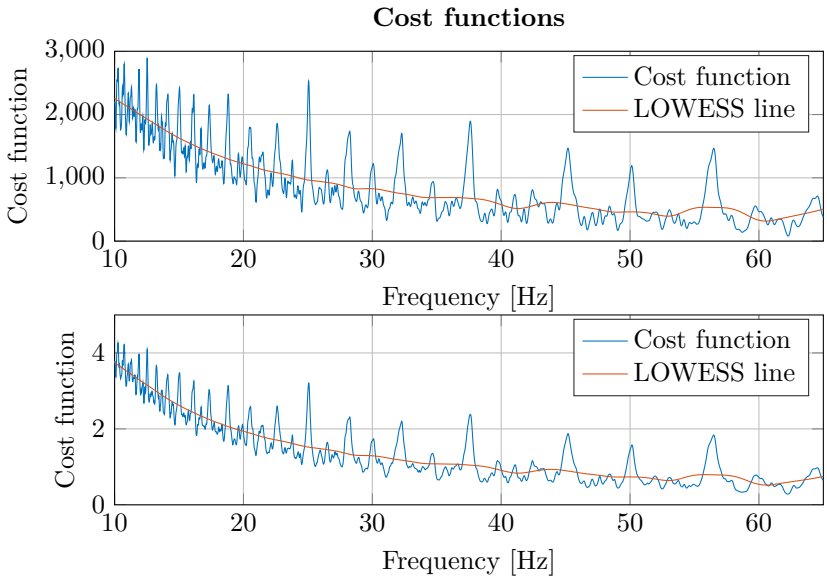

Figure 5.3: Cost function calculated for boat 1. The blue line represents the cost function, while the orange line is the LOWESS line.

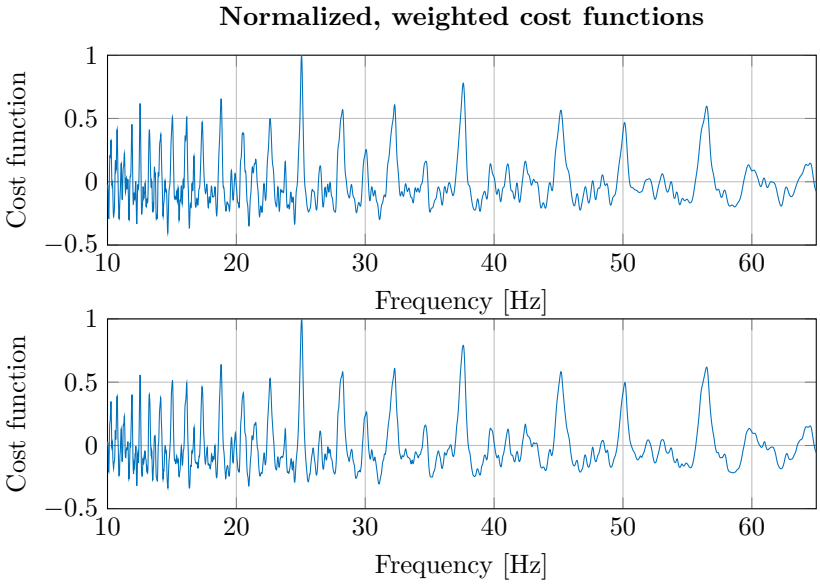

Figure 5.4: Normalized, weighted cost functions calculated for boat 1. The upper plot shows the cost function for NLS, while the lowermost plot shows Capon.

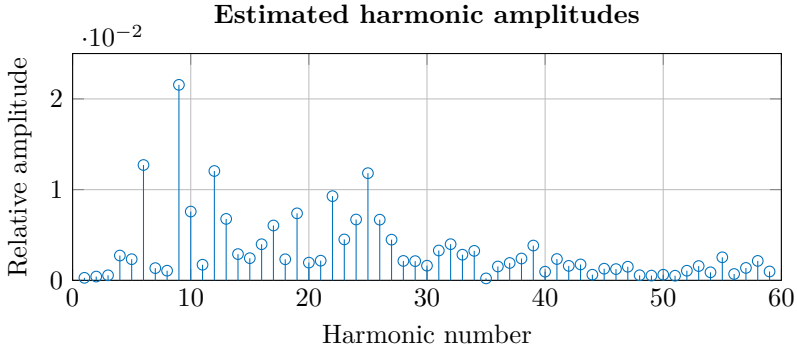

Figure 5.5: Harmonic amplitudes of snapshot 150 for boat 1 calculated using equation 3.2.

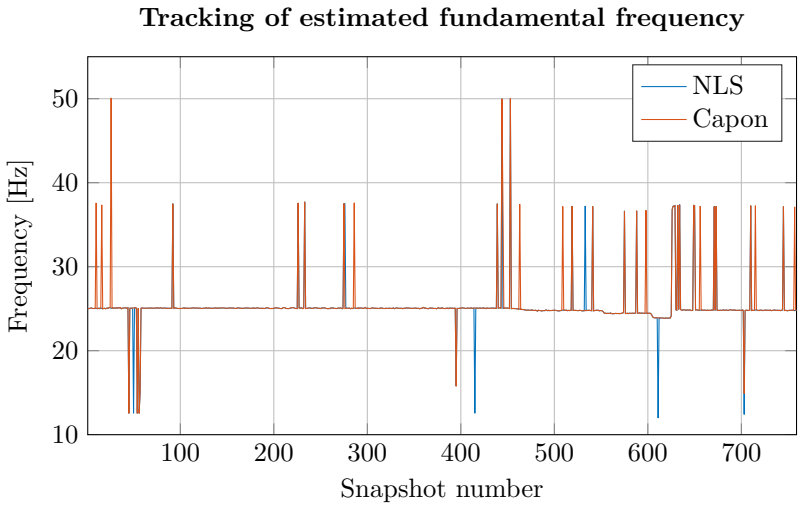

Figure 5.6: Tracking of fundamental frequency for boat 1. The blue line illustrates the NLS result, while the orange line indicates that of Capon.

the spectrogram. In the snapshots where there is an estimator miss, we either get a frequency which is $1/2f_1$, $3/2f_1$, or $2f_1$. This is not unexpected, as the cost functions from our estimators are known to have somewhat large values at these frequencies.

Figure 5.7 shows the spectrogram of the second boat with lines indicating the estimated harmonic frequencies. The NLS harmonics are marked with black lines, while the Capon harmonics are indicated by magenta lines. From this figure we can clearly see how the lines fit well onto the harmonic lines in the spectrogram. Snapshot 150 is located about twenty-five seconds into the file, and from the spectrogram in figure 5.7 we can confirm that both estimators hit the fundamental frequency of 25.08 Hz. We can also see that both estimators follow changes in the fundamental. Notice how both estimators pick up the CPA Doppler shift around 75 seconds, and the frequency tracking follows the spectrum for all but 4 snapshots in the region around CPA. In the regions around the Doppler shift, we can see that the estimators get some misses in estimating the fundamental. This is likely due to the noise which appears in the lower is parts of the spectrum; all harmonic lines in frequencies under 150 Hz disappear in the broadband noise, and some of the higher harmonics disappear in the Lloyd's

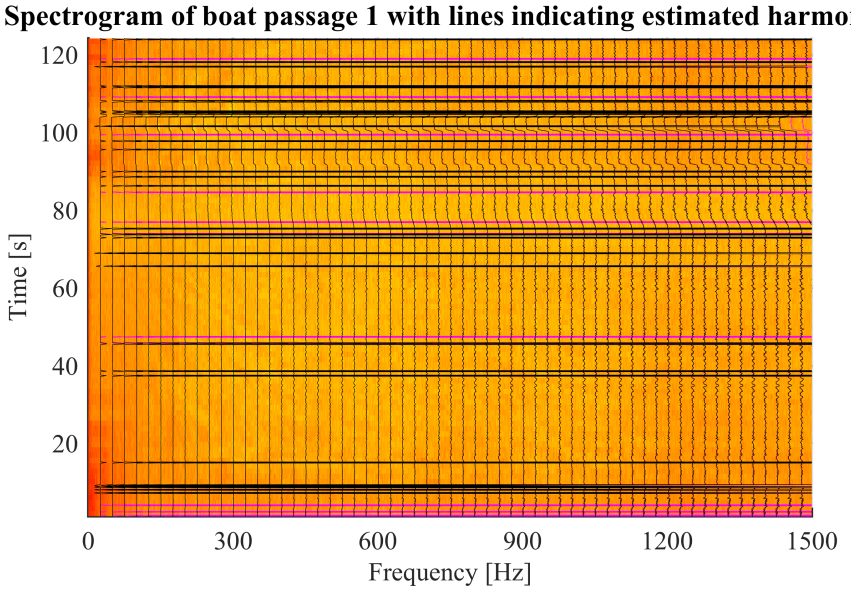

Figure 5.7: Spectrogram of acoustic pressure radiation captured from boat 1. The magenta and black lines indicate harmonic frequencies estimated by Capon and NLS, respectively. See figure 4.1 for spectrogram.

mirror effects around CPA. These effects result in fundamental estimate misses corresponding with both $3/2f_1$ and $2f_1$. By inspecting the estimator results in the region around the fluctuations at 1 minute and 40 seconds, we can see that both estimators can, at least partially, follow the fundamental in the jumps of fundamental frequency. Snapshot 150 is located about twenty-five seconds into the file, and from the spectrogram in figure 5.7 we can confirm that both estimators hit the fundamental frequency of 25.08 Hz.

5.2.2 Boat two

To learn more about the second boat passage, will go through the same procedure as we did to boat 1. Again, we will look into snapshot 150, where both methods estimate a fundamental of 27.89 Hz. Figure 5.8 displays the spectrum of the snapshot. In this spectrum we can see a number of high peaks. The two largest

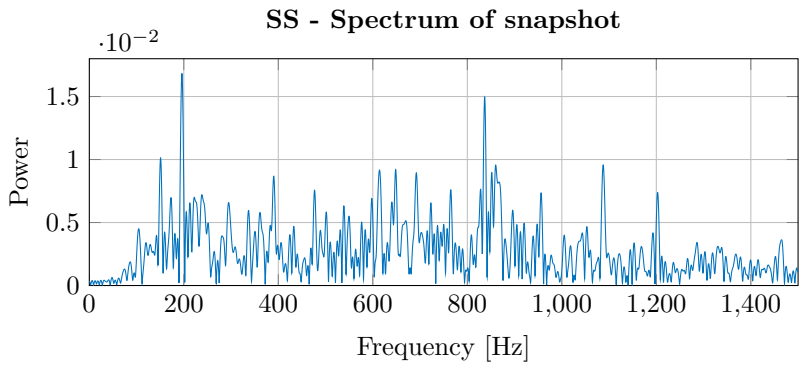

Figure 5.8: Spectrum of snapshot 150 from boat 2.

of these, at 195.9 Hz and 836.8 Hz, correspond with the 7-th and 30-th harmonics, respectively. Like in figure 5.2, we can see that noise in the lower frequencies are strongly dampened. Notice how the power in snapshot 150 is an order of ten higher than the power of this snapshot.

The raw cost functions calculated by NLS and Capon are displayed in figure 5.9. Here we can see that there are local peaks in the areas of the true fundamental, but as in figure 5.3, this peak is a local maximum. Therefore, the subtraction of the LOWESS lines from their respective cost functions is necessary. By comparing these cost functions to those from boat 1, we can see that these have a considerably lower range. The dynamic range in figure 5.9 is 0 to 120 for NLS and 0 to 0.2 for Capon. This likely comes from this snapshot having an order of magnitude lower power than the snapshot from boat 1. It also appears that the NLS cost function has a higher variance around the LOWESS line than the Capon Cost function has around its LOWESS line.

The cost functions modified by subtracting the LOWESS line and normalizing is displayed in figure 5.10. Like we did in figure 5.4, we can see similarities between the NLS and Capon plots, but here we can clearly see that NLS has a slightly higher cost function in areas where we can confirm that the fundamental is not located. Especially the lower frequencies have a higher cost function. Though, this can be expected from hat we could see from figure 5.9, where we saw a higher variance around the LOWESS line in the NLS cost function compared to that of Capon. Since it might also indicate that the difference is frequency dependant, this might be because the LOWESS line follows the Capon line better than the NLS line in this case.

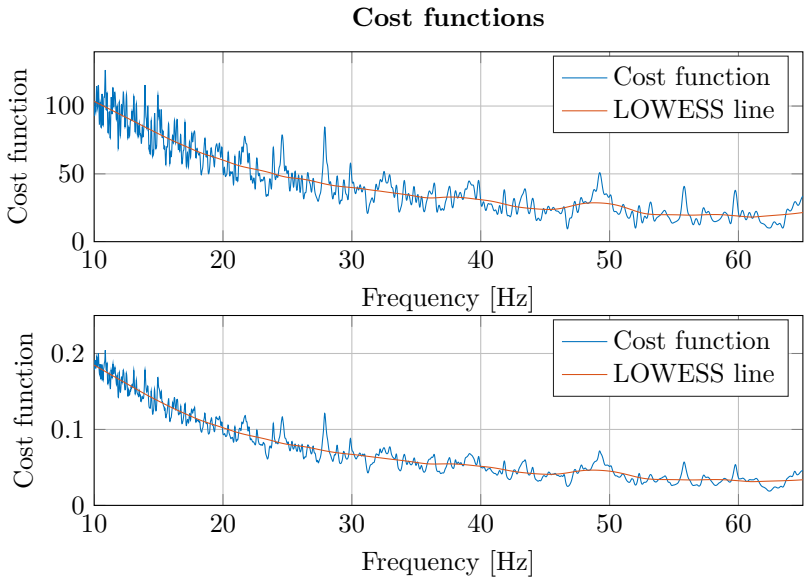

Figure 5.9: Cost function calculated for boat 2. In the upper sub-plot, we can see the graphs for NLS, while Capons are in the lower sub-plot. The blue line represents the cost function, while the orange line is the LOWESS line.

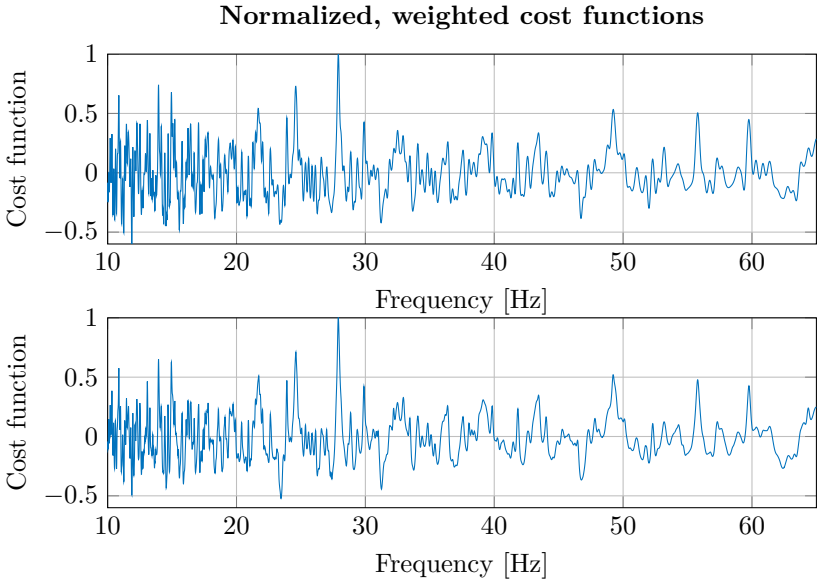

Figure 5.10: Normalized, weighted cost functions calculated for boat 2. The upper plot shows the cost function for NLS, while the lowermost plot shows Capon.

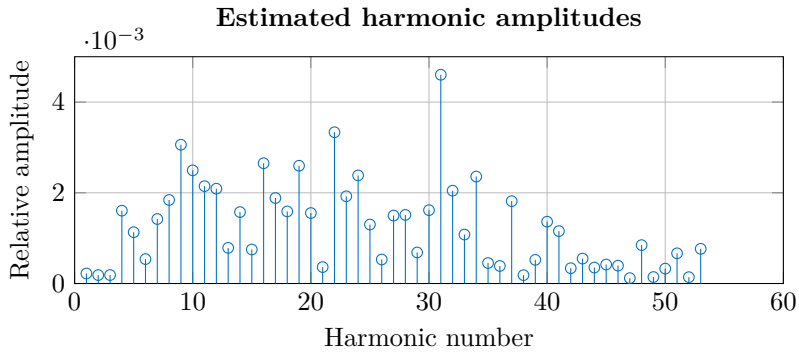

Figure 5.11: Harmonic amplitudes of snapshot 150 for boat 2 calculated using equation 3.2.

The result from applying the estimated fundamental frequency into equation 3.2 to estimate the harmonic amplitudes can be seen in figure 5.11. In this figure, we can see some similarities with the spectrogram.

Finally, to check the performance of the estimators, we introduce figures 5.12 and 5.13. Figure 5.12 shows the frequency tracking of the fundamental frequency estimated using the two methods. From the frequency tracking, we can see that both estimators perform well in the areas with good SNR in the middle, with two misses in between snapshots 100 and 550. Both estimators also follow the subtle frequency shift at CPA, which occurs around snapshot 400. The CPA time seen from the estimator results being around 66 seconds corresponds with what can be extracted from the spectrogram in figure 4.2. We can also see that the estimators fail to get good consecutive estimates for the fundamental frequency after snapshot 700, which is approximately around 116 seconds, and that they fail for multiple snapshots in the range snapshot 550 - snapshot 700. At this point, the boat is starting to disappear in the distance, and we can anticipate that the SNR decreases.

Figure 5.13 shows the spectrogram for boat 2 with lines indicating the estimated harmonic frequencies. The magenta and black lines illustrate NLS and Capon frequencies, respectively. From the spectrogram we can see that the estimated frequency lines fit well onto the harmonic lines for most of the 120 seconds boat passage. By comparing this spectrogram to the one in figure 4.2, we can see that the SNR decreases rapidly after 90 seconds, explaining why the estimator gets such a sudden unstable behaviour.

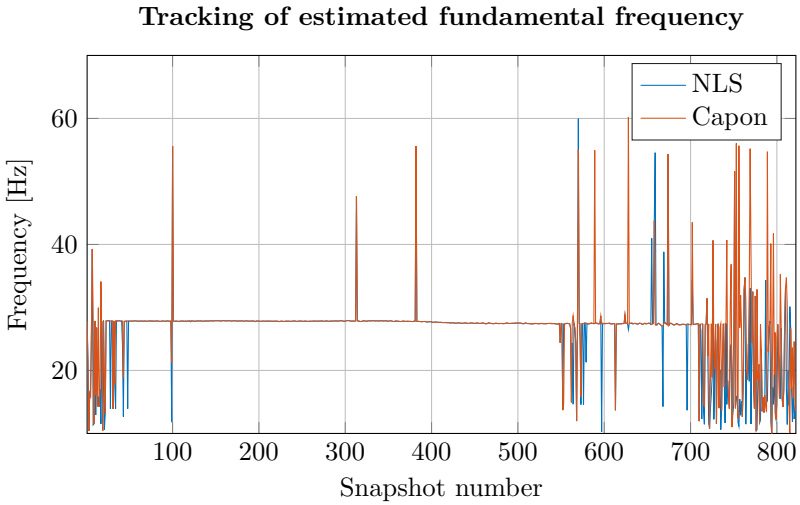

Figure 5.12: Tracking of fundamental frequency for boat 2. The blue line illustrates the NLS result, while the orange line indicates that of Capon.

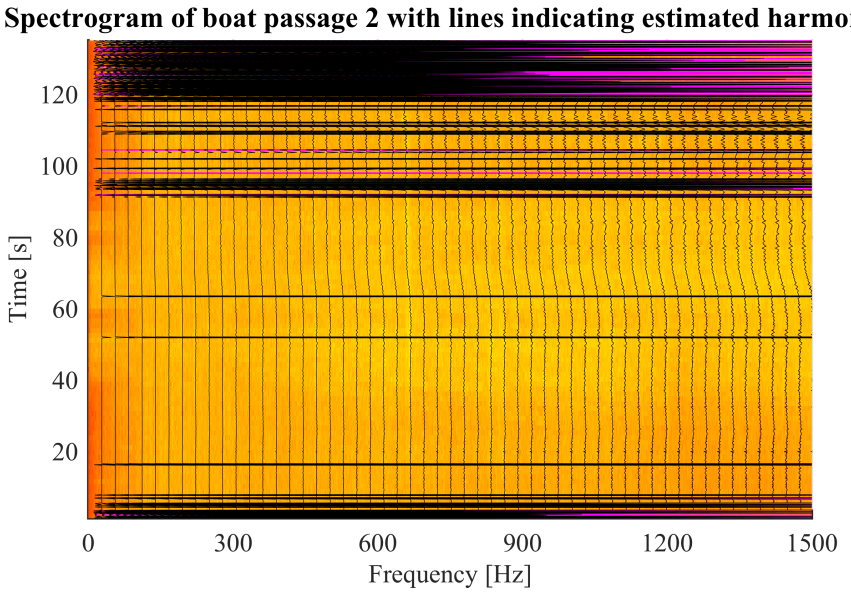

Figure 5.13: Spectrogram of acoustic pressure radiation captured from boat 2. The magenta lines indicate harmonic frequencies estimated by Capon and the black lines those of NLS. See figure 4.2 for spectrogram.

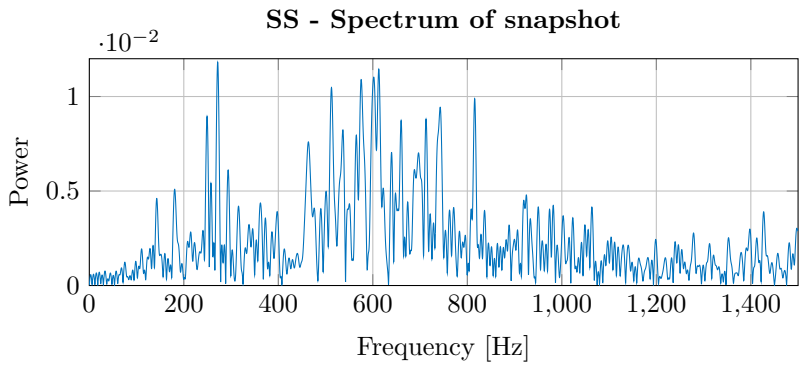

Figure 5.14: Spectrum of snapshot 1050 from boat 3.

5.2.3 Boat three

Boat passage three yields some interesting properties that the prior two did not. By looking at snapshot 1050, which is near the middle of the recording, we investigate this passage further. The spectrum of the snapshot is shown in figure 5.14. As we can see in this figure, there is a large amount of noise between 400 Hz and 900 Hz.

The raw cost functions with LOWESS lines of snapshot 1050 from boat 3 is displayed in figure 5.15. In this figure, we can see that there are no major peaks in any of the cost functions. This confirms that the estimators are having a hard time finding a harmonic series. Recall how we stated in section 4.2.3 that the passage recording had issues with broadband noise in the frequencies between 400 and 900 Hz. Because of this issue, we would have to apply additional signal processing to the data prior to performing an estimation.

Figure 5.16 shows estimated harmonic amplitudes for snapshot 1050. From the figure, we can clearly see that harmonics 14 - 26 have higher amplitudes. With the estimated fundamental of 33.9 Hz these harmonics represent the frequency range 470 - 890 Hz, and corresponds with observation from the spectrum in figure 5.14.

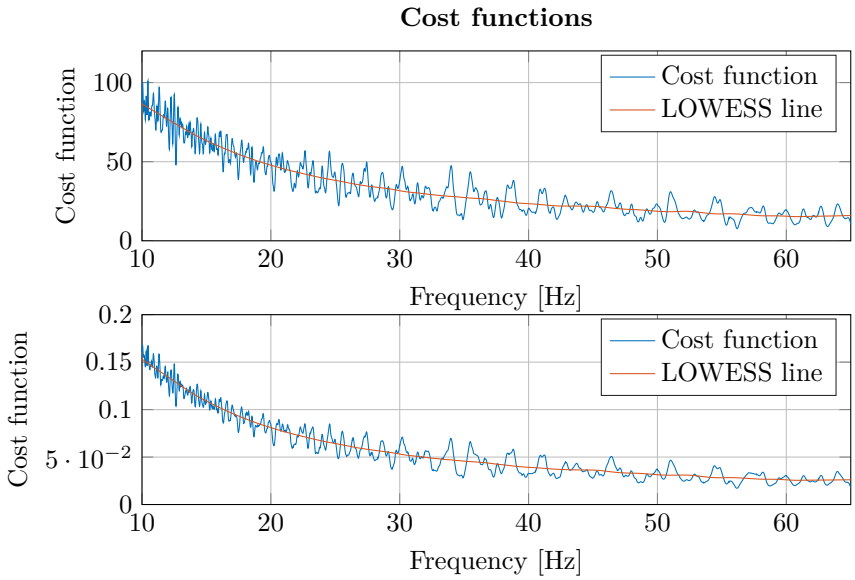

Figure 5.15: Cost function calculated for boat 3. In the upper sub-plot, we can see the graphs for NLS, while Capons are in the lower sub-plot. The blue line represents the cost function, while the orange line is the LOWESS line.

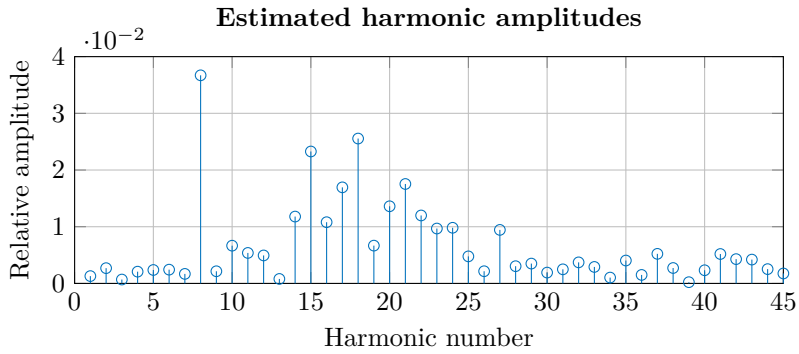

Figure 5.16: Harmonic amplitudes of snapshot 1050 for boat 3 calculated using equation 3.2.

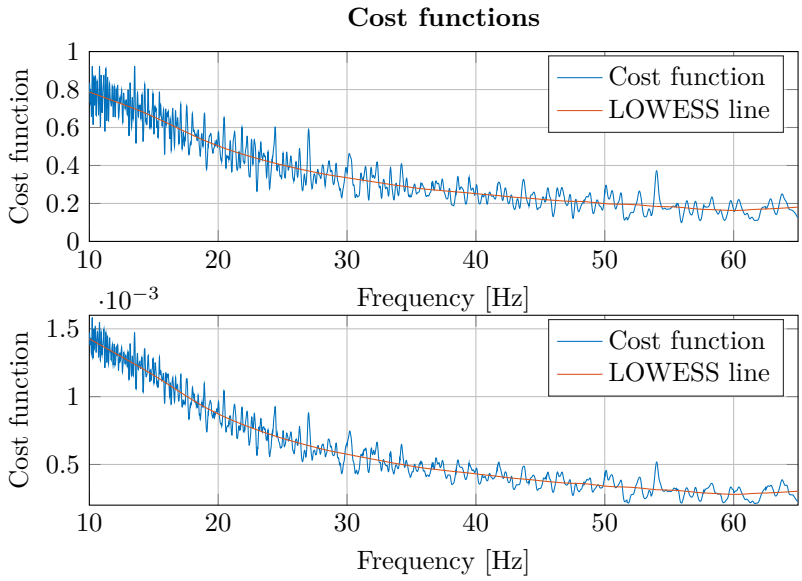

Figure 5.17: Cost function calculated for snapshot 150 of the ambient noise. In the upper sub-plot, we can see the graphs for NLS, while Capons are in the lower sub-plot. The blue line represents the cost function, while the orange line is the LOWESS line.

5.2.4 Ambient noise

Figure 4.4 in section 4.2.4 shows the spectrum of the ambient noise in the datasets forth data sample. Figure 5.17 shows the raw cost functions and corresponding LOWESS lines for snapshot 150 of the ambient noise. These plots show that the cost functions calculated from ambient noise are considerably lower than those in figures 5.3, 5.9 and 5.15. From comparing the cost function in figure 5.17 with those in 5.3 and 5.9, we can also see that there are no obvious harmonic series. Furthermore, we can also notice that the form of the cost function from the ambient noise appear very much like that in figure 3.2, where we investigated the result form applying our estimators to white noise.

Table 5.3: Estimated fundamental frequencies and raw cost function values for boat passages (1-3) and for ambient noise (4).

Number	$J_{NLS,max}$	$J_{Capon,max}$	$f_{NLS,1}$ [Hz]	$f_{Capon,1}$ [Hz]
1	2896.6	4.2668	25.059	25.070
2	126.67	0.2045	27.897	27.897
3	101.03	0.1679	33.991	33.969
4	0.9232	0.0016	13.520	27.017

5.3 Summary of results

Table 5.3 displays the maximum values of the raw cost functions. This shows that there is a large difference between the cost function values we get from ambient noise and ship noise. These result indicate that we can discriminate between cost functions with and without clear harmonic noise.

From table 5.3 we can see a clear difference in the peak values of the raw cost functions. Recall how the CPA distances in table 4.1 was 71.74 meters and 294.65 meters for boat passages 1 and 2, respectively. The difference in maximum raw cost function peaks value between these two boat passings is therefore intuitive as the signal of the latter has propagated further, thus yielding a lower SNR, even though boat two has a higher speed than boat 1.

Table 5.3 also lists the estimated fundamental frequencies by the two estimators. From the first two samples we can see that the estimators hit at frequencies which are close to each other, and in the region of the actual fundamental. For the third boat passage we can also see that the estimators hit approximately the same fundamental frequency. Though, this one is a bit higher than the actual fundamental, which resides around 22.6 Hz in this time region. Lastly, the estimators output different fundamentals for the last file, which contains ambient sound.

Chapter 6

Discussion

In this thesis, we have evaluated the NLS and Capon estimators from (Faltin, 2014), where we implemented the estimators and tested them against synthetic noise. We have rewritten our Capon estimator for an entirely real signal, as this is what our dataset includes. Since we can assume a real signal, and therefore a symmetric autocorrelation matrix, $\boldsymbol{R}$, the Capon estimator computation introduced by (Christensen et al., 2007) can be simplified with equation 3.23. This enables faster computation, as we can compute a larger portion of the total equation outside of the loop for varying fundamental frequency.

We have applied two fundamental frequency estimators to the *Vealøs 2014* dataset gathered with the hydrophone sensor on the FFI developed NILUS underwater measurement node. We recognize that the weighted signal model proposed in the preliminary project, (Faltin, 2014), to handle the decreasing frequency content amplitude in the harmonic series of small boats is unnecessary in this case; data gathered using the hydrophone sensor is already processed in such a way that these problems are reduced by its transfer function. What proved to be a real issue with the dataset is the unknown number of harmonics. We handled this by assuming an upper limit of possible harmonics, and calculate how many harmonics each fundamental in ζ allow within the Nyquist rate.

Raw cost functions calculated by our estimators are problematic, as figures 5.3, 5.9, and 5.15 show. Their shape appear very similar to the graph of assumed number of harmonics in figure 3.1, indicating correlation. This problem was solved by applying local linear regression to the cost functions, and subtracting the resulting LOWESS line. By doing this, we achieve a weighted cost function which fits better with what is expected as output from the estimators. The LOWESS line corrected cost functions presented in figures 5.4 and 5.10 show that we get cost functions with a clear maximum value. We can also see that the cost functions from the two different methods are very similar, and we can state that the methods result in nearly identical cost functions.

The problem with correlation between number of harmonics and the raw cost

functions could also have be solved by calculating with a set number of harmonics, but this would require a very fine balance between number of harmonics and the range of search frequencies in ζ. It is therefore optimal to have a variable number of harmonics. However, if we had more knowledge about the possible range of fundamental frequencies for small boats, a set number of harmonics might have been a valid method, especially if this range is considerably smaller then what we have assumed in this thesis.

We decimated the dataset used in this thesis by a factor of three before dividing it into snapshots for calculation, effectively reducing the Nyquist rate to 1.5 kHz. In certain cases, this can be a problem as some boats may have signature harmonics in frequencies above 1500 Hz. However, with the hydrophone sensor filtering away most frequency contents over 2 kHz, decimation with a factor of three works well for our estimators. This is possible because the estimators do not rely on accurate pressure data, but rather good SNR, such that there is no reason to compensate for the filter in the hydrophone sensor.

The broadband noise in the third data sample shows a possible result of relying on a filter like that of the hydrophone sensor for this type of dataset. In this sample, there is a considerable amount of broadband noise in the filters passband. This leads to the Lloyd's mirror effect having a very strong presence in the total received sound. There are a number of ways we could have bypassed this in order to get results from this data sample. The most obvious are applying a bandstop filter to suppress the problematic frequency range, or decimating with a higher factor. Decimating with a higher factor would also improve the computation time, and is certainly an interesting solution if this should have been implemented into a low power device, as it would both conserve power and omit problems arising from the regions where the hydrophone sensor has its strongest amplification. The fact that a case like the third boat passage can occur in the same dataset as the first and second passages show that this kind of estimator relies on substantial testing before a final implementation. Filtering away certain frequencies would also limit the number of harmonics in the snapshot, and would therefore also affect the estimators.

We have to take figure 5.1 into consideration; here we can see that the Capon estimator can achieve up to 10 percent more hits in the regions below 0 dB SNR. This figure clearly shows that the Capon estimator outperforms the NLS estimator in the aspect of hit percentage. Table 5.2 lists the average computation time for each method in the calculations used to generate figure 5.1. For the considered snapshot length, $N = 500$, we can see that the NLS estimator is faster than the Capon estimator with 5.71 seconds against 34.95 seconds. This implies that the NLS estimator can calculate with larger snapshots, and thus tackle lower SNR, while still processing the data faster. This is a key result in

this thesis, and corresponds with what we experienced in (Faltin, 2014, p. 18), where the computation time of the NLS estimator with a snapshot length of 840 was faster than that of the Capon estimator with a snapshot length of 420.

Results from frequency estimators have shown that they are accurate. The spectrograms with lines indicating harmonic frequencies, as seen in figures 5.7 and 5.13, show that there are large regions with consecutive estimator hits. What we can see from these spectrograms, is that as long as the estimators are stable for consecutive snapshots, the lines match with the harmonic lines in the spectrogram. The frequency tracking plots presented in figures 5.6 and 5.12 show that the majority of estimator misses result in frequencies that are 1/2, 3/2, and 2 multiples of the true fundamental. This suggests that a logical filter, like that proposed in section 3.4 can be utilized to smooth the frequency tracking from these estimators.

The numbers presented in table 5.3 suggest our estimators can both detect small boats, and calculate their fundamental frequency. Detection can be done since the cost functions of snapshots with harmonic noise can be discriminated against those without by comparing their maximum values.

Chapter 7

Conclusion

Throughout the thesis we have introduced the major problems we faced when taking on the challenge of applying fundamental frequency estimators to a real, authentic dataset. We have done this by continuing the work in (Faltin, 2014), with the Non-linear Least Squares, and Capon estimators. The continuation of the work includes rewriting the Capon estimator to handle real signals more effectively.

From the results presented, we can clearly state that the NLS estimator is the best choice for an implementation into a system. With the possibilities it introduces with the estimated harmonic amplitudes, longer snapshot lengths, and shorter computation time, it certainly outperforms the Capon estimator. However, the Capon estimator performs slightly better at estimating the correct fundamental frequency in the synthetic tests presented in section 5.1. The advantage we can see in performance at these low SNRs does not weigh up for the longer computation time the estimator uses.

Both estimators can do their intended job for the straight-forward parts of the dataset, in boat passages 1 and 2, but they prove to have a hard time with boat passage 3, which contains some additional broadband noise which clutters the signal too much for both estimators. We can also see that the estimators can be utilized to detect if there is a source (small vessel) present in water from comparing cost function levels of the samples with and without a source.

Both the NLS and Capon estimators we have presented in this thesis can be implemented with regards to a dataset which is similar to the one we have used by utilizing our advises. A complete such system could recognize harmonic noise, and estimate its harmonic signature.

References

Aster, R. C., Borchers, B., & Thurber, C. H. (2011). *Parameter estimation and inverse problems* (2e ed.). Academic Press Inc.

Christensen, M. G., Stoica, P., & Jensen, S. H. (2007). The multi-pitch estimation problem: Some new solutions. *IEEE International Conference on Acoustics, Speech, and Signal Processing*, *3*(1), 1221-1224.

Faltin, O. G. M. (2014, December). *Analysis of harmonic signatures in underwater noise* (Tech. Rep.). Norwegian University of Science and Technology.

Hovem, J. M. (2012). *Marine acoustics - the physics of sound in underwater environments* (1st ed.). Peninsula Publishing.

Kay, S. M. (1993). *Fundamentals of statistical signal processing* (1st ed.). Prentice Hall.

Nehorai, A., & Porat, B. (1986). Adaptive comb filtering for harmonic signal enhancement. *IEEE Transactions on Acoustics, Speech and Signal Processing*, *34*, 1124 - 1138.

Ogden, G. L., Zurk, L. M., Jones, M. E., & Peterson, M. E. (2011). Extraction of small boat harmonic signatures from passive sonar. *Journal of the Acoustical Society of America*, *129*(6), 3768 – 3776.

Petersen, K. B., & Pedersen, M. S. (2012, nov). *The matrix cookbook.* Technical University of Denmark. Retrieved from `http://www2.imm.dtu.dk/pubdb/p.php?3274` (Version 20121115)

Smistad, R., Buen, H., & Tollefsen, D. (2014). *Måling og analyse av støy fra fritidsbåter* (Tech. Rep.).

Sorensen, E., Ou, H. H., Zurk, L. M., & Siderius, M. (2010). Passive acoustic sensing for detection of small vessels. In *Proceedings of oceans 2010 seattle 20-23 september 2010* (p. 696 - 703). Institute of Electrical and Electronics Engineers (IEEE).

Stoica, P., & Moses, R. (2005). *Spectral analysis of signals* (1st ed.). Pearson Prentice Hall.

Wise, J. D., Caprio, J. R., & Parks, T. W. (1976). Maximum likelihood pitch estimation. *IEEE Transactions on Speech and Signal Processing*, *24*, 418 – 423.

Appendix A

NLS estimator Matlab Implementation

```
function [NLSprod1,wNLSprod1] = NLS_impl8(xx,Zetat,LL,Nsnap,spann)
%   NLS_impl8.m
%   Ole Faltin, electronics student at NTNU, as part of the
%   projectEstimation of harmonic signatures in underwater noise
%   from small boats
%   Masters Thesis for FFI - Dag Tollefsen
%   06.06.2016
%
%   Method proposed by
%   Christensen, M. G. and Stoica, P. and Jensen, S. H.
%   The Multi-Pitch Estimation Problem: Some New Solutions
%   IEEE International Conference on Acoustics, Speech, and Signal
%   Processing, 3(1), 1221-1224.
%
%   NLS Estimator implementation
%   Calulates the fundamental frequency and the cost function.
%
%   In:
%   xx    - Signal vector.
%   Zetat - Array of angular frequencies where the fundamental is
%   being searched for.
%   LL    - Number of harmonics in the signal.
%   Nsnap - Snapshot length
%   spann - regression span - 0<spann<=1
%
%   Out:
%   NLSprod1    - Cost function calculated using NLS.
%   wNLSprod1   - Weighted cost function
%
%%%%%%%%%%%%%%%%%%%%%%%%%%%%%%%%%%%%%%%%%%%%%%%%%%%%%%%%%%%%%%%%%%%%%%%%%%%%

NLSprod1 = zeros(length(Zetat),1);
sTYPE = 'lowess';           % Type of smoothing. default: LOWESS

kk = 0;
while kk < length(Zetat)    % Will execute once for each angular f.
    kk = kk+1;
```

```
38      zetakk = Zetat(kk);      % extract current zeta
39
40      ll = 1:LL(kk);           % Make ll for current w - LL(kk)
41
42      % Make Vandermonde matrix
43      ZZ = exp(1j*zetakk*(0:(Nsnap-1)).'*(ll));
44
45      NLSprod1(kk) = xx' * (ZZ  * ZZ') * xx;
46  end
47  NLSprod1 = abs(NLSprod1);
48  % Perform smooting
49  yy = smooth(NLSprod1,spann,sTYPE);
50  wNLSprod1 = (NLSprod1) - (yy);
51
52  end
```

Appendix B

Capons estimator Matlab Implementation

```
function [Caponc1,wCaponc1] = Capon_impl8(xx,Zetat,LL,Nsnap,spann)
%   Capon_impl8.m
%   Ole Faltin, electronics student at NTNU, as part of the
%   project Estimation of harmonic signatures in underwater noise
%   from small boats
%   Masters Thesis for FFI - Dag Tollefsen
%   06.06.2015
%
%   Method proposed by
%   Christensen, M. G. and Stoica, P. and Jensen, S. H.
%   The Multi-Pitch Estimation Problem: Some New Solutions
%   IEEE International Conference on Acoustics, Speech, and
%   Signal Processing, 3(1), 1221-1224.
%
%   Capon estimator implementation
%   Calulates the fundamental frequency and the cost function.
%
%   In:
%   xx    - Signal vector.
%   Zetat - Array of angular frequencies where the fundamental is
%   being searched for.
%   LL    - Number of harmonics in the signal.
%   Nsnap - Snapshot length
%   spann - regression span - 0<spann<=1
%
%   Out:
%   Caponprod1  - Cost function calculated using Capon.
%   wCaponprod1 - Weighted cost function
%
%%%%%%%%%%%%%%%%%%%%%%%%%%%%%%%%%%%%%%%%%%%%%%%%%%%%%%%%%%%%%%%%%%%%%%%%%%%%

% Common parameters
Caponc1 = zeros(length(Zetat),1);
sTYPE = 'lowess';

RR = acorrmat(xx);          % Requires acorrmat.m

```

```
38  [EVEC,EVAL] = eig(RR);       % Eigen decomposition; assume real xx
39  EPROD = EVEC * diag(1./sqrt(diag(EVAL)));
40
41  kk = 0;
42  while kk < length(Zetat)     % Will execute once for each angular f.
43                               % w in Zetat
44      kk = kk+1;
45      zetakk = Zetat(kk);          % extract current zeta
46      ll = 1:LL(kk);
47
48      % Make signal model for current w
49      ZZ = exp(1j*zetakk*(0:(Nsnap-1)).'*(ll));
50
51      % Calcualte product and take trace
52      Y3 = pinv(ZZ' * EPROD * (ZZ' * EPROD)');
53      Caponc1(kk) = abs(trace(Y3));
54  end
55
56  % Perform smooting
57  yy = smooth((Caponc1),spann,sTYPE);
58  wCaponc1 = (Caponc1) - (yy);
59
60  end
```

Appendix C

Autocorrelation matrix implementation - acorrmat.m

```
function [RR] = acorrmat(xx)
%   acorrmat.m
%   Ole Faltin, electronics student at NTNU, as part of the project
%   Estimation of harmonic signatures in underwater noise from
%   small boats
%   Masters Thesis for FFI - Dag Tollefsen
%   11.05.2015
%
%   Autocorrelation matrix implementation
%   Calcualtes the autocorrelation matrix of a signal snapshot.
%
%   In:
%   xx - Signal snapshot vector. Should be real.
%
%   Out:
%   RR - Autocorrelation matrix.
%
%%%%%%%%%%%%%%%%%%%%%%%%%%%%%%%%%%%%%%%%%%%%%%%%%%%%%%%%%%%%%%%%%%%%%%%%%%%%%%%

%   Common parameters
Nsnap = length(xx);          % Length of snapshot
mx = mean(xx);               % Mean value of snapshot
rr = zeros(1,Nsnap);         % Row vector for top row results

%   Calculation
for k = 0:(Nsnap-1)
    r = 0;
    for n = 1:Nsnap-k        % Correlation
        r = r + sum((xx(n)-mx)*(xx(n+k)-mx)');
    end
    rr(1,k+1) = r;
end

%   Generate first collumn.
cc=[rr(1),conj(rr(2:Nsnap))].';

%   Use toeplitz.m to generate proper RR = autocorrelation matrix.
```

```
38  RR = toeplitz(cc,rr);
39
40  end
```